ENG 324-(EQC 2001/470)

Earthquake design procedures for rectangular underground structures

John Wood

ENG
32a

JOHN WOOD
CONSULTING

Earthquake Commission Research Foundation

EARTHQUAKE DESIGN PROCEDURES FOR RECTANGULAR UNDERGROUND STRUCTURES

EQC Project No 01/470

Prepared: J H Wood

Rev A: 30 June 2004

John Wood Consulting
20 A Ngaumatau Road
Point Howard
LOWER HUTT

Summary

Methods for undertaking the earthquake design of rectangular underground structures have been investigated. In most rectangular underground structures the racking deformations produced by waves propagating in a direction perpendicular to the longitudinal axis are the most critical action and previous studies indicate that vertically propagating shear waves are the predominant wave form governing the design of cross-sections for racking deformation.

The empirical relationship developed by Wang (1993) for assessing the racking interaction of rectangular structures with the surrounding soil during earthquakes was verified by undertaking a large number of simplified dynamic finite element analyses, and by comparison with analytical expressions recently published. The work of Wang was extended by undertaking a large number of simplified dynamic finite element analyses to determine the sensitivity of his interaction curves to variations in the main parameters. This produced a number of charts that can be used in the earthquake design of smaller underground structures where the site information is unlikely to be known in sufficient detail to warrant more sophisticated analyses. The finite element method developed for the present study can also be used directly to analyse large or more complex structures when more detailed site information is available.

Application of the Wang design method to several box culverts and pedestrian subway structures showed that the internal forces from earthquake induced racking deformations can be large in comparison to actions produced by gravity and water pressure loads. It was concluded that these earthquake induced deformations need to be considered in the design of most underground rectangular structures.

Contents

SUMMARY .... **I**

1. INTRODUCTION **1**

2. EARTHQUAKE DAMAGE TO UNDERGROUNGD STRUCTURES **6**

3. PREVIOUS RESEARCH **8**

4. PROJECT SCOPE **12**

5. ANALYSIS METHOD **14**

5.1 FREE-FIELD STRAIN 14
5.2 STRUCTURE STIFFNESS AND FLEXIBILITY 18
5.3 SOIL-STRUCTURE INTERACTION 19

6. RESULTS OF ANALYSES **25**

6.1 COMPARISON OF R VERSUS F_R RELATIONSHIPS 25
6.2 INFLUENCE OF COVER DEPTH 25
6.3 INFLUENCE OF LAYER DEPTH 28
6.4 INFLUENCE OF STRAIN FIELD 28
6.5 INFLUENCE OF STRUCTURE SHAPE 28
6.6 INFLUENCE OF SOIL POISSON'S RATIO 34
6.7 FORCES IN BOX STRUCTURAL MEMBERS WITHOUT SOIL INTERACTION 34
6.8 FORCES IN BOX STRUCTURAL MEMBERS WITH SOIL INTERACTION 37

7. WORKED EXAMPLES **43**

8. CONCLUSIONS **55**

9. ACKNOWLEDGEMENTS **55**

10. REFERENCES **56**

1. INTRODUCTION

Although many rectangular underground concrete structures have strength reserves that apparently lead to satisfactory performance during earthquakes there is considerable uncertainty in engineering design communities in both New Zealand and overseas as to how to estimate the magnitude of the dynamic earth pressures or the shear strain deformations that they are subjected to during earthquakes.

Many technical papers and design codes address the design and analysis of buildings and above-ground structures for earthquake resistance. In contrast, there is significantly less information available for the design of underground structure. Within the past 30 years, particularly since the availability of commercial finite element software, analysis procedures have gradually evolved for most forms of underground structures but to date there have been few published design guidelines and most national and international design codes developed for seismically active countries do not consider underground structures. Analyses and design of large under-ground structures has tended to be carried out on a one-off basis with design criteria developed for each specific project. Considering the variability in ground conditions often encountered in urban areas and the relatively few large underground structures constructed, the lack of the development of a more standardised approach is perhaps not unexpected. However, for many smaller structures such as culverts, services tunnels, and pedestrian sub-ways, which are becoming more prevalent as urbanisation restricts the construction of open channels and above ground development, it is not economical to undertake detailed one-off analyses. There is a need for simplified analysis procedures, design guidelines and code design criteria for these structures. Simplified analysis procedures are also helpful for checking the results of the more sophisticated numerical analyses employed for large underground structures.

Seismic design of underground structures is either omitted completely or not covered adequately in New Zealand design codes. For example, the current Transit New Zealand Bridge Manual identifies the problem of the seismic design of underground structures for culverts and subways with moderate depths of cover but suggests using an out-of-date analysis procedure know as the "stresses at infinity method". Many small underground structures exist in urban areas in New Zealand, for example there are about 13 underground subways, box culverts and highway underpasses in the Lower Hutt City area located in sediments close to the Wellington Fault. None of these have been specifically designed for earthquake effects.

Large underground car-parking buildings and buildings with significant underground basement structures have been constructed in the major New Zealand cities. For these major underground structures seismic effects have usually considered in the design but the analyses have been based on a simplified theory developed for retaining walls with the wall top at the ground surface and the foundation assumed to be rigid. When the structure is constructed below the surface in deep soil layers these simplified methods have obvious limitations. Ultimate strength analysis refinements are leading to less reserve of strength in more complex box and rectangular shapes used in large underground structures. Because of these advancements, underground structures are becoming more vulnerable to earthquake damage and it is therefore important to develop a rational method of defining the earthquake-induced pressures and deformations.

Underground structures are constrained by the surrounding soil or rock and cannot move independently so are not generally subjected to significant dynamic amplification effects. They are affected by the deformation of the surrounding ground and not by the inertia forces acting on the structure. In contrast, surface structures often have natural frequencies that are within the range of the predominant frequencies of earthquake ground motions resulting in resonant effects with the accelerations acting on the structure amplified with respect to the ground surface to produce large inertia forces. Constraint effects of the ground on underground ground structures and amplification of acceleration on above ground structures are main factors that have contributed to the generally better performance in major earthquakes of underground structures than above ground structures.

The earthquake response of underground structures is usually considered with reference to the following three principal types of deformations:

- Axial
- Curvature
- Racking (rectangular cross-sections) or ovaling (circular cross-sections)

As shown in Figure 1.1 axial and curvature deformations develop when seismic waves propagate either parallel or obliquely to the longitudinal axis of the structure. The general behaviour of a long structure subjected to a component of parallel wave propagation is similar to that of an elastic beam with axial and flexural strains computed by beam theory. In simplified analyses, the structure is assumed to be flexible relative to the surrounding soil or rock and to respond with the same deformation pattern as in the free-field elastic seismic waves. These simplified analyses are often employed for pipelines that have relatively small cross-sectional areas and for the preliminary analyses of tunnels. When the structure is stiff in the longitudinal direction relative to the surrounding soil, it will not be compliant with the soil or rock deformations. For this case, interaction effects need to be considered by employing either numerical methods or approximate solutions developed from wave propagation theory for beams on an elastic foundation.

As shown in Figure 1.2 ovaling or racking deformations develop in an underground structure when the seismic waves propagate in a direction perpendicular or with a significant component perpendicular to the longitudinal axis resulting in distortion of the cross-section. In this case, and for long structures, a plane-strain two-dimensional analysis may be

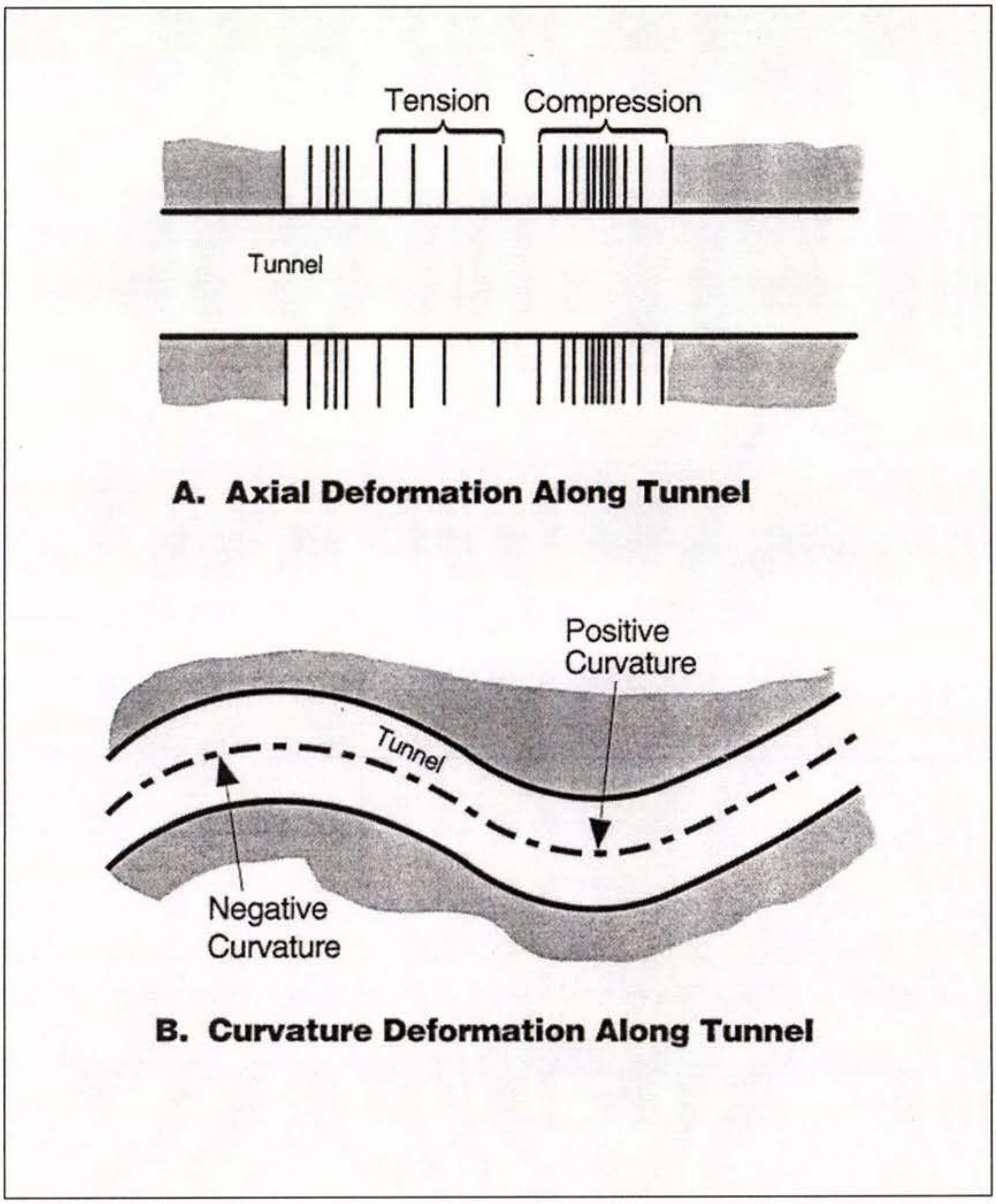

Figure 1.1. Axial and curvature deformations. (Source Owen and Scholl, 1981)

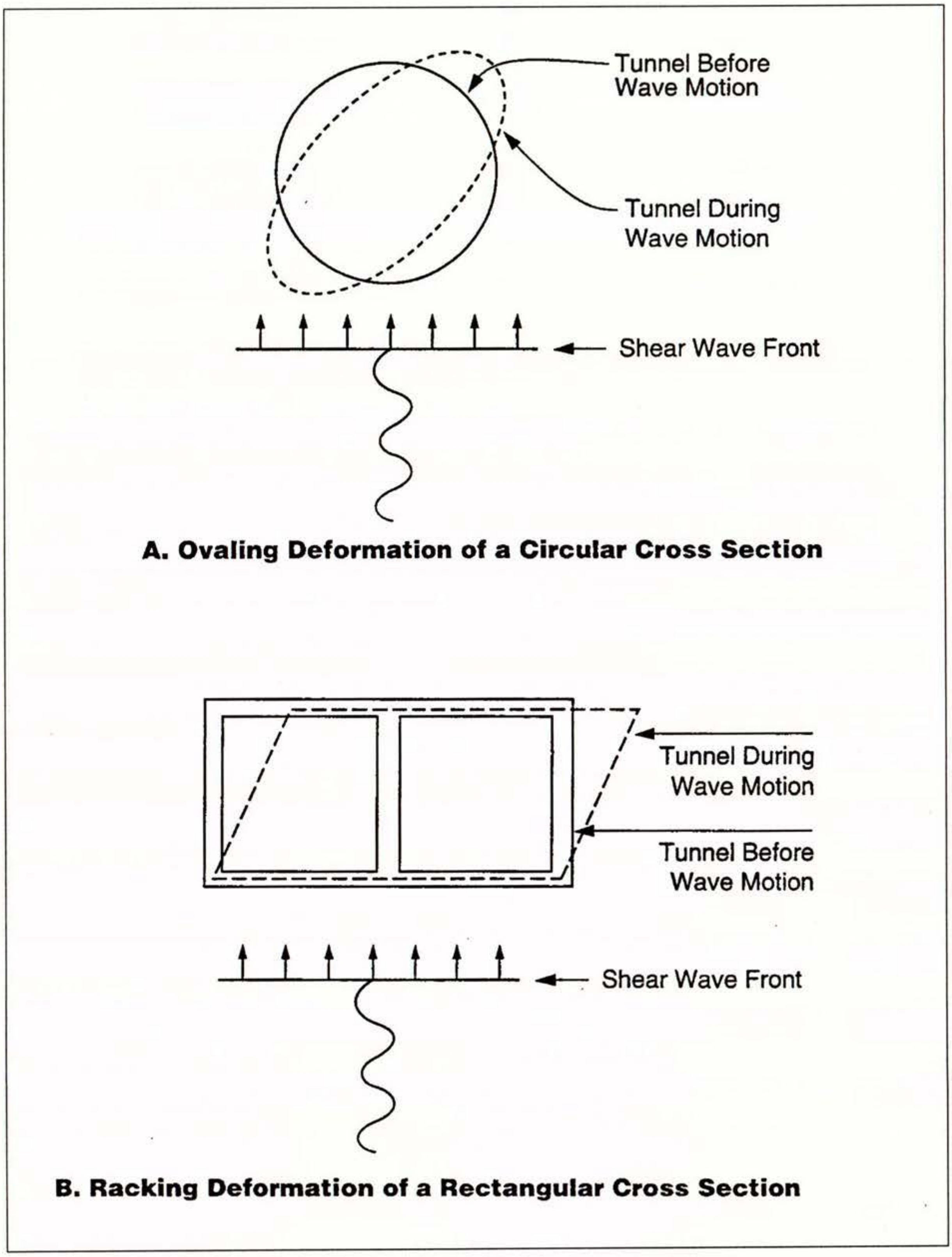

Figure 1.2. Ovaling and racking deformations. (Source Wang, 1993)

employed. Any type of seismic wave propagating in any direction can cause racking or ovaling deformations. However, previous studies indicate that vertically propagating shear waves are the predominant wave form governing the design of cross-sections for ovaling or racking.

Before the development of sophisticated numerical methods, research on the earthquake analysis of underground structures focused on circular cavities in elastic continua and then advanced to consider lined cavities located within elastic half-spaces. Lined circular shapes were a reasonable approximation to typical tunnel cross-sections and could be analysed by analytical theory of elasticity and approximate elasticity methods. Elastic wave theory was also applied to develop procedures for assessing the axial and flexural strains acting normal to the cross-section of long flexible structures. Although the longitudinal analysis of rectangular structures can be carried out using this same elastic wave theory there are no simple analytical procedures that can be used to analyse the cross-sectional deformations. Consequently it has only been with the rapid advance of numerical methods in the last decade that satisfactory analysis procedures have been developed for rectangular structures. Prior to this, rectangular cross-sections were designed by assuming that they were subjected to the free-field soil or rock shear strains and by the application of standard structural frame analysis methods. Rectangular underground structures are suitable for cut-and-cover construction and are therefore often constructed close to the surface in relatively soft soils. In this situation, the assumption of compatibility with the free-field shear strains can lead to very conservative designs.

2. EARTHQUAKE DAMAGE TO UNDERGROUNGD STRUCTURES

Published research on the past performance of underground structures and openings during earthquakes has been summarised by Wang (1993). Research reports and papers by Dowding and Rosen (1978), Owen and Scholl (1981), Wang (1985) and Sharma and Judd (1991) are mentioned in his summary. The Sharma and Judd study extended Owen and Scholl's work and collected qualitative data for 192 reported observations from 85 world-wide earthquakes. Sharma and Judd correlated the vulnerability of underground facilities with six factors: overburden cover, rock or soil type, peak ground acceleration (PGA), earthquake magnitude, epicentral distance and type of lining. The main findings from this work were:

- Damage decreases with increasing overburden depth.
- More damage occurred in facilities constructed in soil than in competent rock.
- For PGA's less than 0.15 only 25% of the cases reported damage. For PGA's greater than 0.15 g, 69% of the cases reported damage.
- More than 50% of the damage reports were for earthquakes with magnitude M exceeding 7.
- Facilities were most vulnerable when within 25 to 50 km of the epicentre.
- The proportion of damaged cases of concrete-lined tunnels was greater than for unlined cases. This was attributed to the poor ground conditions that originally required the openings to be lined.

Of particular relevance to the present study was the damage to rectangular underground structures in the 1971 San Fernando earthquake. Owen and Scholl (1981) reported damage to five cut-and-cover conduits, and culverts with reinforced concrete linings, with failure of longitudinal construction joints, cracking and formation of plastic hinges at the top and bottom of the walls. Lew et al (1971) reported severe damage to box culvert sections of the Wilson Canyon flood control channel. A large underground reinforced concrete reservoir, part of the Balboa Water Treatment plant, suffered severe damage. The walls, roof slab, floor slab and some of the columns of this 150 m x 150 m x 11.5 m high reservoir were extensively damaged. It was thought that the damage was related to settlement and sliding produced by the ground shaking but soil shear strains and earthquake-induced pressures on the walls were significant factors (Priestley et al, 1986).

Six underground stations out of the total of 21 subway stations in the Kobe area were severely damaged in the 1995 Hyogoken-nanbu earthquake. Sections of tunnels connecting the damaged stations and the tunnel section of the Hanshin Railway sustained damage (Iwatate et al 2000). The damaged structures were constructed by the cut-and-cover method. A large number of the central reinforced concrete columns of twin cell structures were cracked and in one case the columns failed with collapse of the roof and a 2.5 m subsidence of the street above. The primary factor believed to have caused the damage and failures were large shear distortions of the box structures induced by shear strains in the surrounding ground during the earthquake. The failed central columns had insufficient ductility to withstand the distortions imposed upon them.

Less serious damage to underground common utility boxes and parking structures in Kobe was also reported (PWRI 1996).

In relation to the Kobe damage, Nishiyama et al (2000) stated that the damage to cut-and-cover tunnels and subways was unexpected as they had been considered to be relatively safe from earthquake effects compared to above ground structures. Apparently, except for important facilities and those constructed in soft ground, seismic design is not specifically considered for underground structures in Japan. Because of the damage, a number of research programmes have recently been initiated and the seismic design of these structures will undoubtedly receive greater attention in future.

In the 1999 Chi Chi, Taiwan, earthquake a large partially underground rectangular concrete tank at the Taichung County Water supply treatment plant was extensively damaged with a large section of the roof collapsing (Brunsdon, 1999). Causes of the damage are unknown but it is likely that earthquake-induced pressures on the walls were a significant factor.

3. PREVIOUS RESEARCH

Much of the past research reported in the literature on the seismic analysis of underground structures has often been overly theoretical and difficult to implement in design applications or has been orientated towards a specific structure. There is available a considerable volume of published work related to circular tunnels and pipelines but there is little information on how this work might be relevant to structures with rectangular cross-sections.

Kuesel (1969) presented design recommendations for underground rectangular subways that were developed for the design of the San Francisco Bay Area Rapid Transit System (BART). His work was a pioneering development that produced the first published design recommendations sufficiently versatile and simple enough to gain acceptance over a range of applications in varying soil conditions. Kuesel used conventional wave propagation theory to estimate the curvature and shearing distortion strains to be applied to the structures. His method did not include soil-structure interaction affects and so was only strictly applicable to very flexible structures in relation to the surrounding soil. In relation to the BART structures, he concluded that most had sufficient capacity to absorb the imposed distortions elastically, and no special provisions need be made for seismic effects. Where plastic deformations were indicated, the design criteria that he developed included special structural details to provide the required ductility.

In reviewing Kuesel's work, Wang (1993) stated that some of the soil deformation profiles and other assumptions were applicable only to the BART project. However the design philosophy and the general approach proposed was still valid, even when viewed more than two decades later.

Hwang and Lysmer (1981) reported a complex numerical study to evaluate the soil-structure interaction effects on the response of large underground rectangular to travelling seismic waves. By including interaction effects this work was a significant advancement on the work of Kuesel. To demonstrate the application of their work they analysed a specific structure. However, they did not vary the critical parameters to any extent and it was not possible to apply their findings to design applications without repeating detailed numerical work. Hwang and Lysmer concluded that for large structures, although the interaction effects on the computed ground surface motions were small, the presence of the structure significantly reduces the computed strains because the rigidities of the structures provide significant resistance to deformation. It was therefore overly conservative to design to the strains developed in the free field. They further concluded that the assumption of vertically propagating waves lead to errors in predicting the stresses and strains induced in underground structures. However, the results from their example showed that the simplification of using vertically propagating waves, instead of the more correct assumption of travelling waves, gave conservative estimates of the stresses in the plane of the cross-section.

For the Los Angeles Metro project, Monsees and Merritt (1991) developed design criteria using the Kuesel free-field deformation method for estimating the racking deformations of underground rectangular structures. Their criteria permitted joints to be strained into the plastic range under the Maximum Design Earthquake (MDE) provided that no plastic hinge combinations were formed that could lead to a potential collapse mechanism.

To develop a simple and practical procedure for use in design of rectangular underground structures that accounted for soil-structure interaction effects, Wang (1993) carried out an extensive parametric study using dynamic soil-structure interaction finite element analyses. His work was limited to investigating the racking effects produced on the cross-sections of typical rectangular shaped elastic frame structures with rigid joints under vertically propagating shear waves. Two horizontal earthquake accelerograms were input to rigid bases underlying the soil strata to simulate the vertically propagating shear waves. Five different one and two barrel structural configurations were considering with differing height to width ratios of the cross-sections. The average shear modulus of the soil was varied to provide six different homogenous soil profiles and one with the soil shear modulus linearly increasing with depth. Four different depths of soil cover to the top of the structures were investigated.

Dynamic finite element analyses were performed for 25 cases of the soil-structure interaction system with varying combinations of the soil profile, structure configuration and input ground motion. For each of the 25 cases a free-field site response was performed, followed by a corresponding soil-structure interaction analysis.

To present his results in a convenient and compact form, Wang defined a flexibility ratio as the structure racking flexibility divided by the shear flexibility of the area of soil displaced by the structure (see Section 5.3). The racking flexibility, which is the displacement at the top of the structure divided by the structure height for a unit horizontal force applied at the top of the structure, was found by simple frame analysis or alternatively from closed form solutions derived for single barrel structures and the soil shear flexibility from the soil strata input data. He also defined a racking coefficient as the ratio of the racking displacement of the structure embedded within the soil layer per unit height, divided by the free-field soil shear strain averaged over the height of the structure. The racking coefficient was calculated from the results of the free-field and soil-structure interaction finite element analyses.

Further details of Wang's analyses and design method are presented in Section 5.3.3 below. Results of his analyses are shown in Figure 5.7 where his structure racking coefficients, R, are plotted against flexibility ratios, F_r and comparisons are made with other closed form solutions presented in the research literature and some of the results of the present study.

An interesting result of Wang's study was that points from his numerical analyses plotted very closely along the normalised R versus F_r curves obtained for circular lining cross-sections from closed form solutions.

The main conclusions from Wang's work were:

- Taking into account soil structure-interaction effects is important when the flexibility ratio, F_r, is significantly different from 1. When F_r is less than one, the conventional design methods (no interaction) will be too conservative, and when F_r is greater than one, the conventional method will underestimate the displacement response of the structure.
- The normalised R versus F_r curve is reasonably insensitive to the structure geometry.
- The normalised R versus F_r curve is reasonably insensitive to the input ground motion characteristics, and also the absolute stiffness and stiffness variation details of the soil profile. (These parameters obviously influence the free-field shear distortions, which need to be estimated by a suitable method to enable the absolute values of the structure racking deformation to be calculated.)
- The normalised R versus F_r curve is reasonably independent of the depth of burial when the soil cover exceeds the structure height.

Although further research on underground rectangular structures has been undertaken since the publication of Wang's 1993 monograph on seismic design of tunnels it still remains the most comprehensive guideline document for seismic design of underground structures.

Nishiyama et al (2000) and Iwatate et al (2000) report recent Japanese research on subway structures. Both studies were related to underground rail station subway structures that failed in the 1995 Hyogoken-nanbu earthquake. In both projects, shaking table model investigations and numerical analyses were undertaken. The results from these studies indicated that there are a wide range of parameters that need to be considered in analysis of structures of his type. Although the results were not been presented in a suitable form for design application they will be useful for verification of future numerical studies.

Wood and Jenkins (2000) used an elastic finite element dynamic analyses method to investigate earthquake-induced forces in the cross-sections of buried arch structures. They assumed a rigid base beneath the arch foundation soil layers and a response spectrum modal analysis procedure was used to calculate the actions in the arch. A particular shortcoming of this approach was that the significant level of "radiation damping" arising from the wave energy reflecting out through the boundaries of the model could only be estimated. The results of the analyses indicated that dynamic amplification in the soil strata surrounding the arch could in some cases produce much larger arch actions than estimated by simple static design procedures.

Penzien (2000) used an approximate theory of elasticity method to evaluate the racking deformation of rectangular and circular tunnel linings including soil-structure interaction effects. The method followed the procedure used by Penzien and Wu (1998) for circular linings. Because the dimensions of a typical tunnel cross-section are small compared with the wavelengths in the dominant ground motions producing the racking deformations, Penzien assumed that the cross-section was interacting with soil in a uniform strain field. He further assumed that because the inertia forces from the lining and surrounding soil, as produced by interaction effects, are small, that a quasi-static analysis procedure could be used. A further approximation used for the rectangular cross-section was the neglect of the normal stresses that occur on the soil/structure interface. Penzien's work resulted in the development of simple closed form expressions for the racking ratio R in terms of the flexibility ratio F_r previously defined by Wang. By defining R for a circular cross-section as the ratio of the principal diameter strain for the lining and the imaginary circle in the free field, and using generalised lining and soil stiffness parameters, Penzien indicated that the expression was identical for both the circular and rectangular cross-sections. He also found good agreement between his expression and the numerical results of Wang (1993).

Nishioka and Unjoh (2002 and 2003) presented simplified analysis and design procedures for underground rectangular structures. By undertaking both numerical analyses, and theoretical derivations based on a dynamic substructure method, for rectangular cross-sections, they developed an empirical expression for the racking ratio R in terms of a structure to soil flexibility ratio. Both these ratios were defined to be essentially identical to those used by Wang (1993). Their numerical work was based on the dimensions of typical common utility boxes (CBU's) located in Kobe. Some of the structures analysed received minor cracking damage in the 1995 Hyogoken-nanbu earthquake. Nishioka and Unjoh extended the work of Wang by considering the nonlinear response of the structure and proposing a design method based on limiting the shear deformation to an acceptable value determined by a nonlinear push-over analysis of the structure in which plastic hinges formed at the critical joints.

Comparisons of the Nishioka and Unjoh R versus F_r relationship with the Penzien (2000) relationship and the Wang (1993) numerical results are shown in Figure 5.7

4. PROJECT SCOPE

Originally it was planned to determine the racking distortions in rectangular cross-sections of underground structures by undertaking sophisticated dynamic finite element analyses generally following the methods described by Wang (1993). However, following the completion of a literature review it was clear that considerable numerical work had been carried out by Wang and that his work had been verified by similar sophisticated numerical studies more recently completed by Nishioka and Unjoh (2002 and 2003). It was decided that there would be little benefit in repeating further complex dynamic finite element analyses.

Trial analyses demonstrated that a simplified pseudo-dynamic finite element procedure, in which the interaction was analysed in the strain field of the first mode of response of a shear layer could be used to accurately study the soil-structure interaction effects, and that a complete analysis of any design problem could be reliably carried out by combing these interaction results with either a numerical or empirical analysis to determine the free-field shear strain response of the soil strata. This simplified interaction method allowed several hundred analyses to be performed to cover a comprehensive range of the soil and structural input parameters likely to be encountered in practise and in this way advanced the design procedures published previously.

The work completed in this project advances previous research by demonstrating that a pseudo-dynamic analysis method, readily amenable to design office application, can be used to calculate the interaction effects. Graphical solutions were also developed that allow the free-field shear distortions to be estimated without the need for numerical analyses. The wide range of analyses completed allow the influence of the following parameters to be independently assessed:

- Cover depth of soil over the structure
- Soil layer depth
- Strain field depth versus shear modulus profile
- Structure geometry
- Influence of soil Poisson's Ratio

One significant shortcoming of the work by Wang and others is that although they provided satisfactory methods of estimating the racking deformation they did not develop satisfactory methods for computing the force actions within the structure. Although the racking deformation is an important result, the bending moments, shear and axial forces within the cross-section (generally represented by a rigid jointed frame) need to be known to calculate the stresses and the magnitude of any inelastic strains in the structural members. Wang suggested an approximate method in which a frame analysis is carried out using either a concentrated force or a triangular load distribution applied to the structure of sufficient magnitude to produce that calculated racking deformation. This procedure requires a detailed frame analysis and does not correctly represent the interaction effects of the soil in this phase of the analysis. In the present study the interaction model was used to compute the frame forces and these are presented in graphical form suitable for preliminary design of major structures and for the complete design of smaller structures.

Application of the study results to the design of rectangular cross-sections, including a method of considering inelastic structural behaviour, is demonstrated by worked examples.

The analysis of the curvature and axial response of long structures has not been considered in the present study. Wang (1993) presents satisfactory design analysis procedures for these deformations in his monograph on seismic design of tunnels.

5. ANALYSIS METHOD

The evaluation of the racking performance of the cross-section of a rectangular underground structure subjected to earthquake ground motions can be undertaken using the following steps:

(a) Evaluation of the free-field peak shear strain in the soil at the average depth of the structure. The free-field is defined here to be a point in the soil sufficiently remote from the structure so that the state of strain is uninfluenced by the structure.

(b) Evaluation of the elastic and post-elastic stiffness of the structure.

(c) Evaluation of the racking deformation of the structure from the free field strain (see Section 5.1), structure stiffness (Section 5.2) and soil-structure interaction curves presented in this report (Section 5.3).

(d) Evaluation of the member forces in the structure (Section 6.).

Details of the methods and procedures available for undertaking the above four steps are given in the following sections.

5.1 Free-Field Strain

The shear distortion of the ground from vertically propagating shear waves is usually considered to be the most critical and predominant effect producing racking type deformations in underground rectangular structures. Numerical analytical methods have often been often applied to estimate the free-field shear distortions, particularly in sites with variable stratigraphy. Computer codes such as SHAKE and FLUSH based on one-dimensional wave propagation theory for equivalent linear systems have been developed to carryout these types of analyses. Most commercially available codes require the site to be simplified into horizontal layers with uniform properties. More sophisticated analysis procedures using nonlinear wave propagation theory are available but have mainly been applied in research rather than in design applications.

In the present study, an alternative to undertaking numerical analysis to predict free-field shear deformations has been developed by evaluating theory of elasticity analytical solutions for vertically propagating shear waves in a layer of uniform thickness. These solutions may provide sufficiently good approximations for design of many smaller underground structures, particularly where the site soil properties are not know in any great detail. They are also helpful in providing quick solutions for preliminary analysis work, and provide a useful verification method for more sophisticated numerical analysis.

Analytical solutions were evaluated for a uniform elastic shear layer of infinite horizontal extent overlying rock assumed to form a rigid lower boundary. Solutions were evaluated for the following depth profiles of the elastic shear modulus, G.

(a) Uniform

(b) Parabolic with the surface value $G_t = 0$

(c) Linear variations with G increasing with depth. The variation of G with depth in the layer was defined by $G(y) = G_b(1 - q\ y/H)$, where G_b is the shear modulus at the base of the layer, y is the height above the base, H is the thickness of the layer and q is a parameter varying between 0 and 1.

Plots of G versus depth for the layers investigated are shown in Figure 5.1. The layers included uniform, parabolic, and linear variations with q = 0.75, 0.95, 0.9 and 0.95. These variations cover the range likely to occur in practise for common geological conditions. For convenience of presentation, all the layers investigated were taken to have an average shear modulus over the layer depth of $G_{ave} = 100$ MPa.

Analytical solutions for normal modes of vibration for elastic shear layers with uniform, parabolic and linear variations of shear modulus with depth are given by Wood (1973). These solutions were used to evaluate first horizontal mode displacement and shear strain responses for typical elastic shear layers with H = 50 m, G_{ave} = 100 MPa, and a uniform density $\rho = 2.0$ t/m^2. First mode displacement and shear strain responses calculated for a one-g static base acceleration are shown for the various layers in Figures 5.2 and 5.3.

First mode periods of vibration for the analysed layers are given in Table 5.1

Table 5.1. First Horizontal Mode Periods of Shear Layer

Layer Description	**Period, T_1** sec
Uniform	0.894
Parabolic	0.811
Linear, q = 1.0	0.826
Linear, q = 0.95	0.819
Linear, q = 0.90	0.818
Linear, q = 0.75	0.826

The response to a dynamic base acceleration input is obtained by scaling the one-g static responses by $Sa(T_1)/g$ where $Sa(T_1)$ is the spectral acceleration of the input acceleration response spectrum at T_1, the first horizontal mode period of the layer.

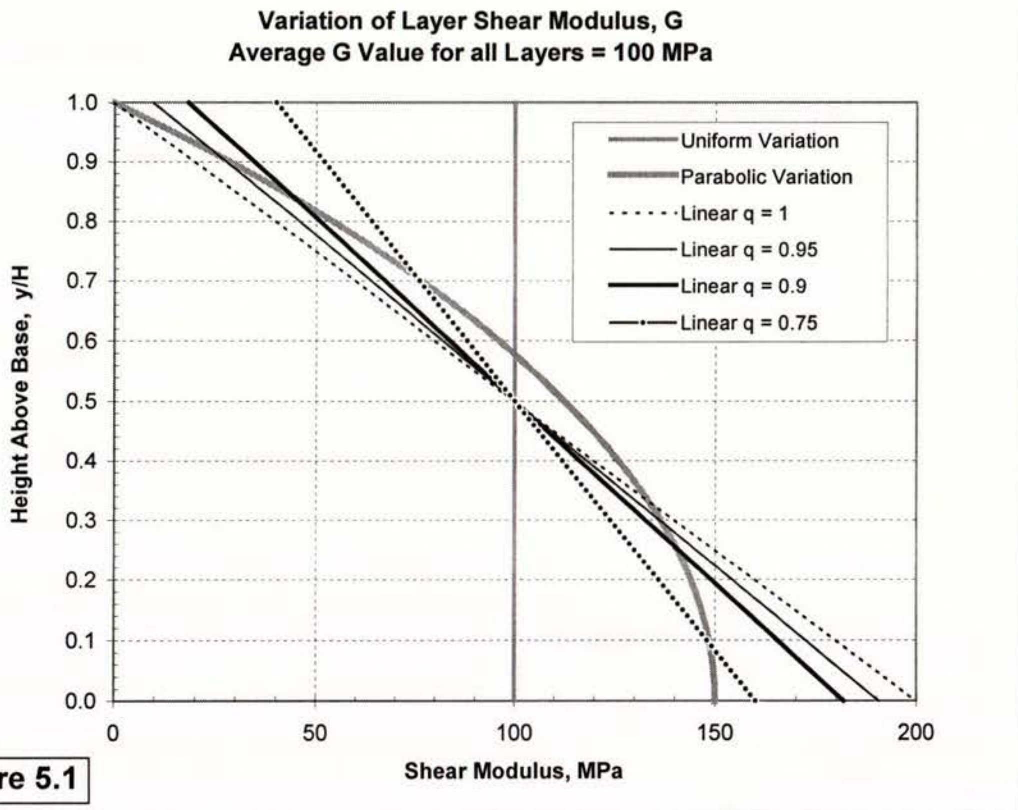

Figure 5.1

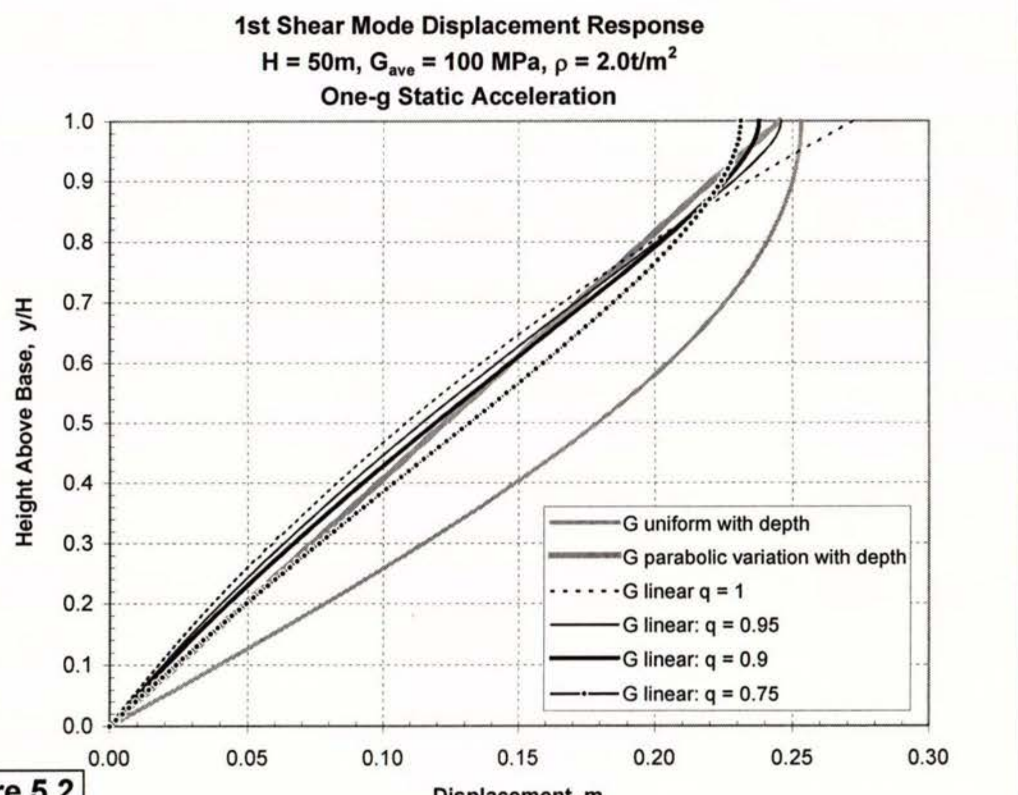

Figure 5.2

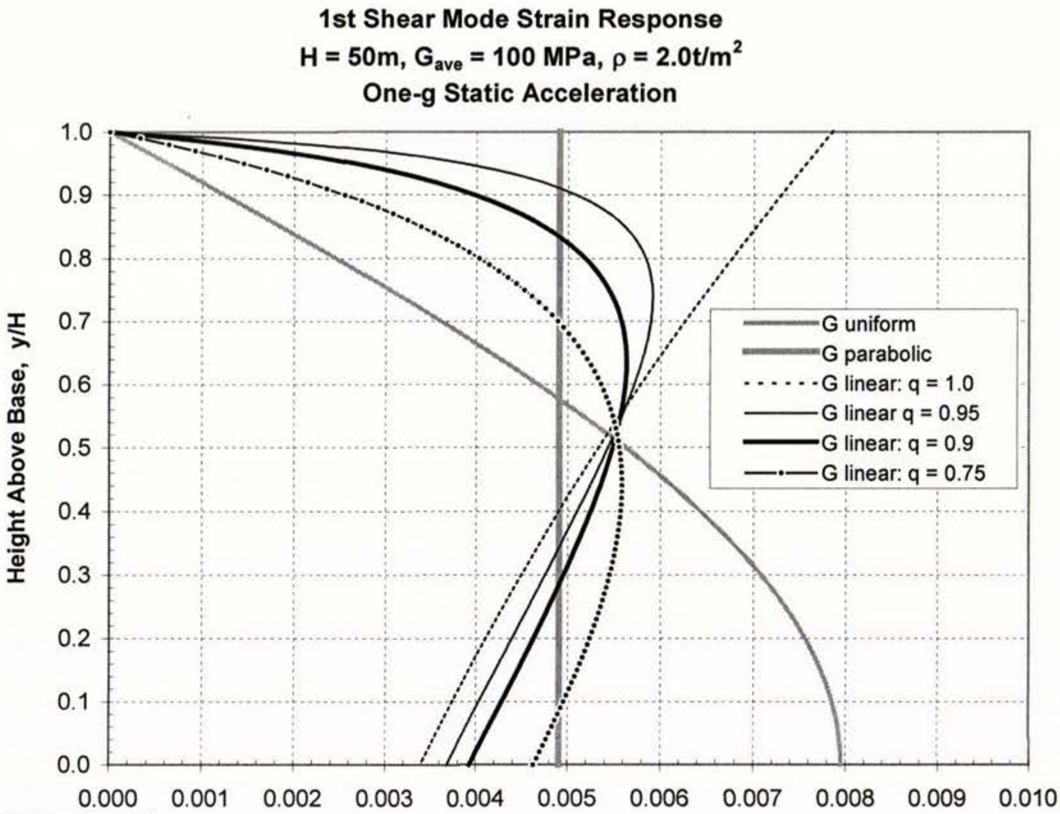

Figure 5.3

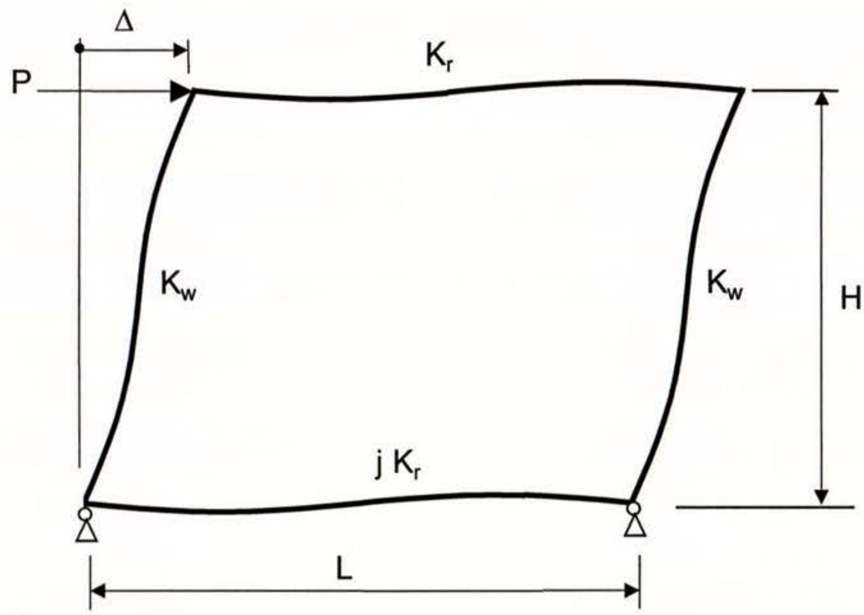

Figure 5.4

It is possible to present the displacement and strain responses and the first mode periods in dimensionless form but it was considered to be more informative to present absolute values for a typical layer. These values can be readily scaled to give the response and periods for a layer of any thickness, average shear modulus or density (assumed uniform). Scaling functions to give the required site values of first mode period, displacement and strain, T_s, u_s, ε_s from the standard layer values presented for the $H = 50$ m, $G_{ave} = 100$ MPa, and $\rho = 2$ t/m^2 layer are as follows:

$$T_s = T_1\left[\frac{H_s}{50}\right]\sqrt{\frac{100\rho_s}{2G_s}} \qquad (5.1)$$

$$u_s = u_1\left[\frac{H_s}{50}\right]^2\left[\frac{100\rho_s}{2G_s}\right] \qquad (5.2)$$

$$\varepsilon_s = \varepsilon_1\left[\frac{100.H_s\rho_s}{50.2.G_s}\right] = \varepsilon_1\left[\frac{H_s\rho_s}{G_s}\right] \qquad (5.3)$$

Where T_1, u_1 and ε_1 are the standard layer values given in Table 5.1, and Figures 5.2 and 5.3

The analytical solutions for the first horizontal mode strain response show that different rates of increase in the shear modulus with depth can produce large variations in the strain profiles. In particular, strains near the surface for a linear increase in G with a low value near the surface can be much higher than is the case for a layer with G uniform over the depth.

5.2 Structure Stiffness and Flexibility

Most underground structures of rectangular shape are designed to act as rigid jointed box structures. The simplest example of this type of structure is the single-barrel box shown in Figure 5.4. To assess the racking stiffness or flexibility, the structure is loaded with a horizontal load P at the roof level to produce a racking or shear deformation of Δ. The structure is assumed to extend sufficiently normal to the plane of the section for plane-strain conditions to exist. Simple closed form solutions for the racking stiffness and flexibility (1/stiffness) for this single-barrel structure have been published previously. (For example, Shepherd and Wood, 1966). The elastic flexibility can be written as:

$$f_{st} = \frac{\Delta}{P} = \frac{H^2}{24K_w}\frac{1}{\left[1 - \frac{2+3r+3jr}{2+2r(2+2j+3jr)}\right]} \qquad (5.4)$$

Where:

$$K_w = \frac{EI_w}{H} \qquad K_r = \frac{EI_r}{L} \qquad r = \frac{K_r}{K_w}$$

E is Young's modulus for the material and I_w and I_r are the moments of inertia per unit length of the wall and roof respectively. H, L and j are defined in Figure 5.4.

If the roof and floor have equal flexural stiffness coefficients (j = 1) then Equation (5.4) reduces to:

$$f_{st} = \frac{H^2}{24K_w}\left[1 + \frac{1}{r}\right] \qquad (5.5)$$

For the case of an infinitely rigid floor, which might be a reasonable approximation for a structure constructed on a rock base, equation (5.4) reduces to:

$$f_{st} = \frac{H^2}{12K_w}\left[\frac{2+3r}{1+6r}\right] \qquad (5.6)$$

There are no simple solutions available for multi-barrel structures but reducing the multi-barrel structure to and equivalent single-barrel structure can provide a good approximation for the stiffness or flexibility. Each wall element of the equivalent single-barrel structure has one-half of the sum of the flexural stiffness of all the wall elements in the multi-barrel structure, and the roof and floor elements of the equivalent structure have the sum of the corresponding roof or floor elements in the multi-barrel structure. Numerical frame analysis indicated that the error from this approximation is less than 6% with the approximation underestimating the flexibility.

For multi-barrel or multi-storey structures with complex geometry, the racking flexibility can be readily computed numerically using conventional frame analysis software.

Under high racking deformations yield in the members may occur leading to plastic hinge formation in the walls, roof or floor members. Progressive development of the hinges can be investigated by a pushover analysis using nonlinear frame analysis software. To investigate the deformation following the formation of sufficient hinges to form a collapse mechanism it is usual to assume bilinear elasto-plastic behaviour.

5.3 Soil-Structure Interaction

Because of both soil-structure interaction and dynamic inertial effects, the soil shear strains in the vicinity of the structure are generally significantly different to the free-field shear strain at the corresponding depth in the soil layer.

A reduction in total mass of the soil and structure at the soil cavity created by the structure may have some influence the inertial forces in the vicinity of the structure, however previous research has concluded that inertial effects do not have a significant impact on the shear strain field. Often the mass change is small in relation to the total mass in the layer corresponding to the height of the structure and acting in unison with the structure during dynamic loading.

In contrast to influence of soil inertial effects, soil-structure interaction effects may produce significant changes in the shear strains near the structure. If a cavity in the soil is unlined, then the shear strains in the soil near the cavity would clearly be greater than the free-field shear strain. If a stiff structure is inserted in the soil cavity then the shear strains may be less than the free-field and conversely with a very flexible structure the shear strains may be greater than in the free-field.

In assessing soil-structure interaction effects on underground structures it is usual to define shear strain deformation and flexibility ratios. The shear strain deformation ratio, R, is defined by:

$$R = \frac{\textit{Shear deformation of structure embedded in soil (including interaction)}}{\textit{Free-field shear deformation over height of structure}}$$

$$R = \frac{\Delta_{sti}}{\Delta_{ff}} \tag{5.7}$$

The flexibility ratio, Fr, is defined by:

$$F_r = \frac{\textit{Shear flexibility of free standing structure without soil interaction}}{\textit{Shear flexibility of soil block of same overall dimensions as structure}}$$

$$F_r = \frac{f_{st}}{f_s} \tag{5.8}$$

Soil shear stiffness is defined by:

$$K_s = G = \frac{\tau}{\gamma}$$

Where G = soil shear modulus in the soil at the level under consideration

τ = soil shear stress

γ = soil shear strain

From the soil shear stiffness definition it follows that the shear flexibility of a block of soil of height H and length L is given by:

$$f_s = \frac{H}{LG} \tag{5.9}$$

The flexibility ratio F_r can be readily computed from the soil shear modulus G and the structure flexibility coefficient f_{st}. (Procedures described in Section 5.2 can be used to compute the structure flexibility coefficient.) Methods for calculating the shear deformation ratio, R, from the flexibility ratio have been investigated in several previous research projects (see Section 3) and also in the present study. The structure shear deformation (including soil-structure interaction) Δ_{sti} can be readily calculated from the shear deformation ratio R and estimates of the peak free-field shear deformation Δ_{ff} during the design earthquake event. The structure shear deformation can then be used to calculate the earthquake-induced forces in the members of the structure. A summary of available methods for determining the shear deformation ratio is presented below.

5.3.1 Penzien Interaction Method

Penzien (2000) derived the following closed form expression for R using an approximate static theory of elasticity method:

$$R = \left[\frac{4(1-\nu_s)}{1+\alpha_s} \right] \qquad (5.10)$$

in which,

$$\alpha_s = (3-4\nu_s)\frac{f_s}{f_{st}}$$

and ν_s is Poisson's ratio for the soil.

The main assumptions made by Penzien in his approximate analysis procedure were:

(a) Uniform strain field

(b) No inertia effects

(c) Plane-strain conditions

(d) Normal stresses acting on the surfaces of the structure ignored.

5.3.2 Nishioka and Unjoh Interaction Method

Nishioka and Unjoh (2002) derived the following closed form expression for R from a finite element approximation:

$$R = \frac{2F_r}{(F_r+1)} \qquad (5.11)$$

The assumptions made were similar to those made by Penzien (2000) but the derivation method was less rigorous. Nishioka and Unjoh (2002) verified expression (5.11) against finite element analyses of a twin-barrel structure of varying stiffness for two different soil stiffness conditions and obtained satisfactory agreement.

Equation (5.10) from Penzien's analysis reduces to Equation (5.11) for Poisson's Ratio, $\nu = 0.5$. Equation (5.11) can therefore be expected to give satisfactory results for some soil properties but may not be satisfactory for soils with low values of ν, particularly when F_r becomes large.

5.3.3 Wang Interaction Method

By undertaking 25 dynamic finite element analyses of typical rectangular structures Wang (1993) showed that the relationship between R and F_r for rectangular structures was closely represented by the following closed form expression derived for circular tunnels:

$$R = \frac{8F_r(1-\nu_s)}{2F_r + 5 - 6\nu_s} \qquad (5.12)$$

Wang's dynamic finite element analyses were performed using the computer code FLUSH (1975), a two-dimensional, plane-strain, finite element program using a frequency domain solution technique. The analyses were based on linearly elastic soil properties and an energy absorbing boundary was used on one side of the mesh to minimise dynamic boundary effects. Two synthetically generated ground input motions were input at the rigid base of the model to simulate vertically propagating shear waves.

Five different single-barrel and twin-barrel box structures were analysed with heights varying between 4.6 to 7.9 m and L/H ratios varying from 1 to 3.5. The soil medium was assumed to be homogenous in 22 of the cases analysed. A soil profile with linearly increasing shear modulus with depth was used for the other three cases. The soil cover over the structures was limited to a range of 4.6 to 6.9 m. A soft soil profile depth of 18.3 m was used with an underlying 6.1 m layer of dense soil above the rigid foundation. An average shear modulus taken at the mid-height of the structure was used to represent the soil stiffness and to calculate the flexibility ratio for these three cases.

5.3.4 Interaction Method Used in the Present Study

In the present study R versus F_r relationships have been developed for a range of structures and site soils conditions by carrying out 200 dynamic finite element analyses. The analysis procedure was similar to that used by Wang but the dynamic analysis process was simplified by undertaking a modal analysis and investigating the strain field in the first mode of each of the layers investigated. This simplification enabled a wide range of the important parameters to be investigated. Good precision was obtained by using a fine element mesh. Because of the dynamic analysis simplification and the refined mesh it was possible to reliably calculate the forces in the members of the rectangular box structure.

Information on the member forces has not previously been published. Wang proposed approximate methods of calculating the forces by a frame analysis procedure based on the interaction shear deformation but this method did not properly account for the soil interaction normal stresses on the members.

The main assumptions made in the finite element analyses carried out in the present project were:

(a) Plane-strain conditions.

(b) Linearly elastic soil and structure material properties.

(c) Dynamic response constrained to the first shear mode of the layer.

The rigid frame single-barrel and twin-barrel box structures with dimensions shown in Figure 5.6 and 5.7 were investigated. Properties and dimensions adopted for the analyses were:

- Material Young's modulus = 20 GPa
- Material Poisson's ratio = 0.2
- All members were assumed to have the same uniform thickness. Thickness values of 200, 250, 300, 350, 400, 500, 600, 700 and 800 mm were used to obtain solutions for a wide range of structural flexibility.

Properties adopted for the soil layer were:

- Layer depths of 20 m and 50 m.
- Shear modulus uniform and parabolic with a value of 40 MPa for the uniform layer and an average value over the depth of 100 MPa for the parabolic layer (150 MPa at the base of the parabolic layer.)
- Soil Poisson's ratio = 0.4
- Depth of cover taken as 5, 10, 15m for both layers. Additional cover depths of 20 m and 45 m were investigated for the 50 m layer. The 45 m cover represents a limiting case of the structure on a rigid foundation under a very deep soil layer.

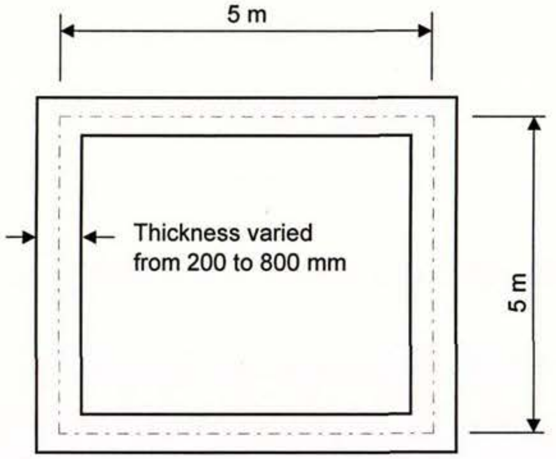

Single-Barrel Structure

Figure 5.5

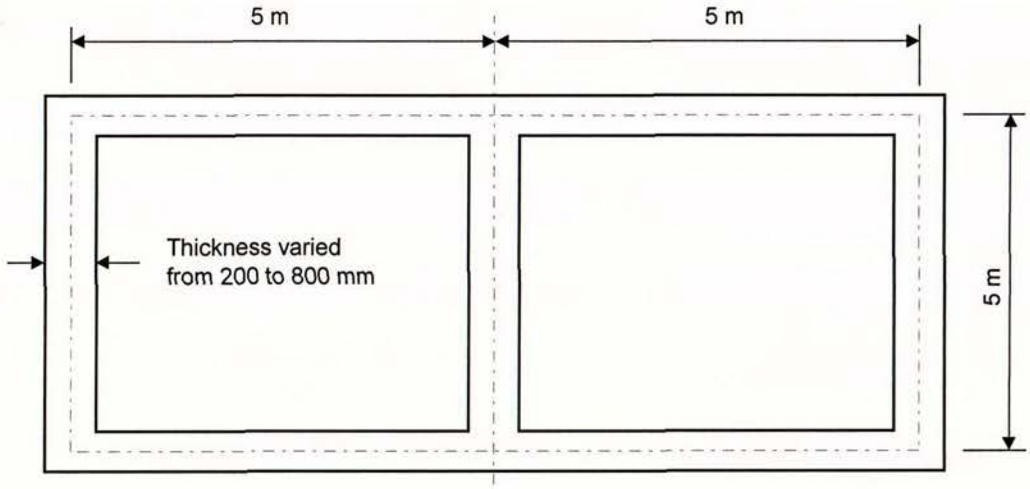

Double-Barrel Structure

Figure 5.6

6. RESULTS OF ANALYSES

6.1 Comparison of R Versus F_r Relationships

R versus F_r curves for the single and twin-barrel structures analysed in the present study are compared with the numerical results of Wang (1993), and the theoretical relationships given in Equations 5.10 (Penzien, 2000), 5.11 (Nishioka and Unjoh, 2002) and 5.12 (Wang, 1993) in Figure 6.1. A soil Poisson's Ratio of 0.4 was used in the present analyses and in the evaluation of the theoretical expressions. The depth of cover for the present analyses was taken as 5 m and the structures were embedded in a 50 m deep soil layer with a shear modulus increasing parabolicaly from zero at the surface.

When the flexibility ratio approaches zero, representing a perfectly rigid structure, the R value also reduces to zero. At F_r = 1, the structure has the same stiffness as the soil and the structure has a similar racking distortion to the ground distortion in the free-field, resulting in an R value of approximately 1.0. When the flexibility ratio is greater than 1.0, the structure is flexible in relation to the ground and the racking distortions becomes magnified with respect to the distortion of the ground free-field distortion.

There is good general agreement between the R versus Fr curves produced by the various methods particularly at Fr ration less than 2.0. At the larger Fr ratios there is some divergence. The Nishioka and Unjoh expression produces strain ratios that are two low when Fr is greater than 2.0; however, as explained in Section 5.3.2 their expression does not contain a Poisson's Ratio term and gives more satisfactory results when Poisson's Ratio is close to 0.5.

6.2 Influence of Cover Depth

R versus F_r curves for the single-barrel structure in the uniform 50 m thick layer are shown in Figures 6.2 and 6.3. Figure 6.2 shows the F_r ratio out to the maximum value investigated of 15 and Figure 6.3 the curves with an expanded scale for F_r from 0 to 2.0.

From the plotted results is apparent that the structure located on the rock base is a rather special case where interaction effects are less pronounced than is the case for the structure in the middle regions of the layer or nearer to the layer surface.

There is little variation between the curves for cover depths between 5 and 20 m. Surface layer effects cause moderate changes in the interaction for shallow covers at high Fr ratios, but once the structure is covered by more than its height of soil, the interaction does not change significantly with increasing depth of the structure within the layer.

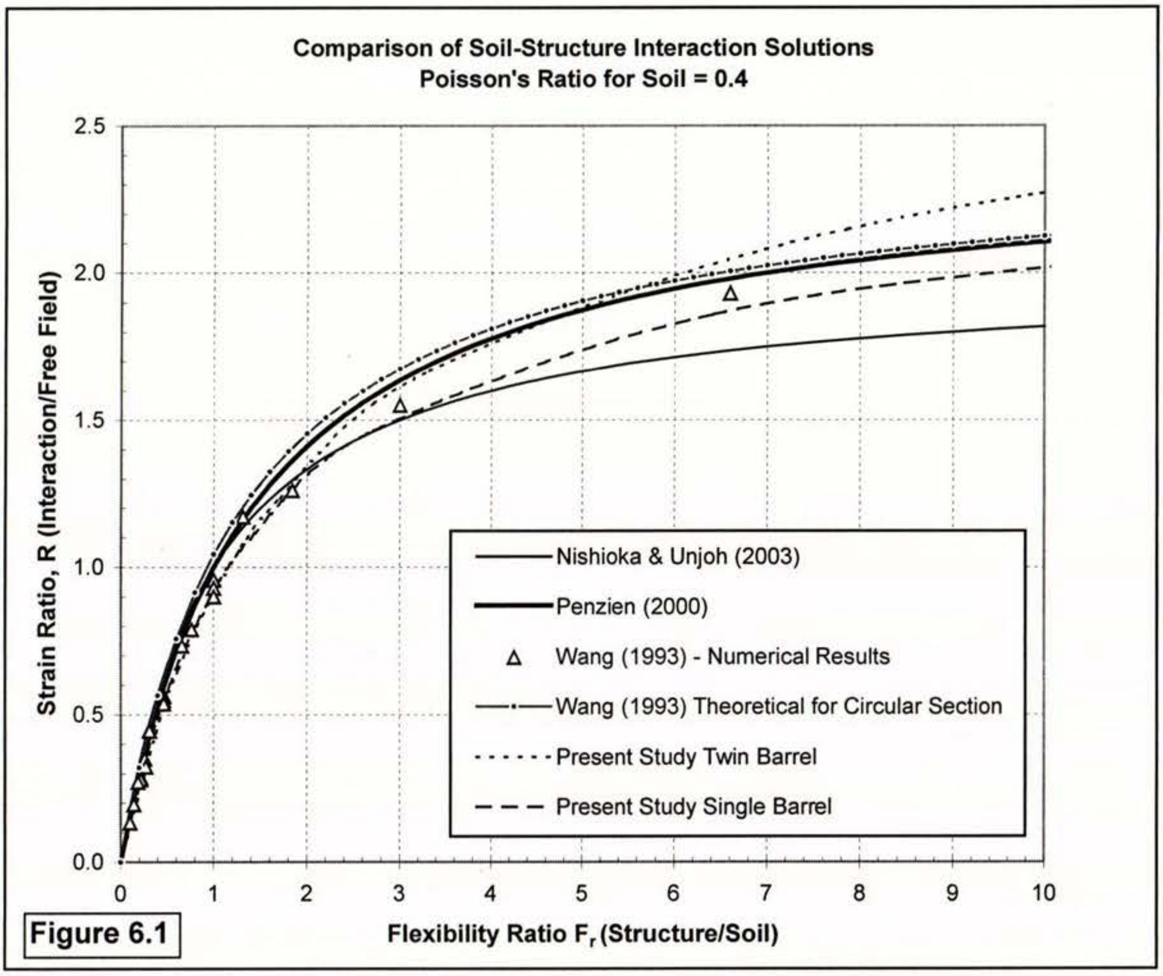
Comparison of Soil-Structure Interaction Solutions
Poisson's Ratio for Soil = 0.4
2.5
2.0
1.5
1.0
0.5
0.0
Strain Ratio, R (Interaction/Free Field)
0
1
2
3
4
5
6
7
8
9
10
Flexibility Ratio F_r (Structure/Soil)
Nishioka & Unjoh (2003)
Penzien (2000)
Wang (1993) - Numerical Results
Wang (1993) Theoretical for Circular Section
Present Study Twin Barrel
Present Study Single Barrel
Figure 6.1

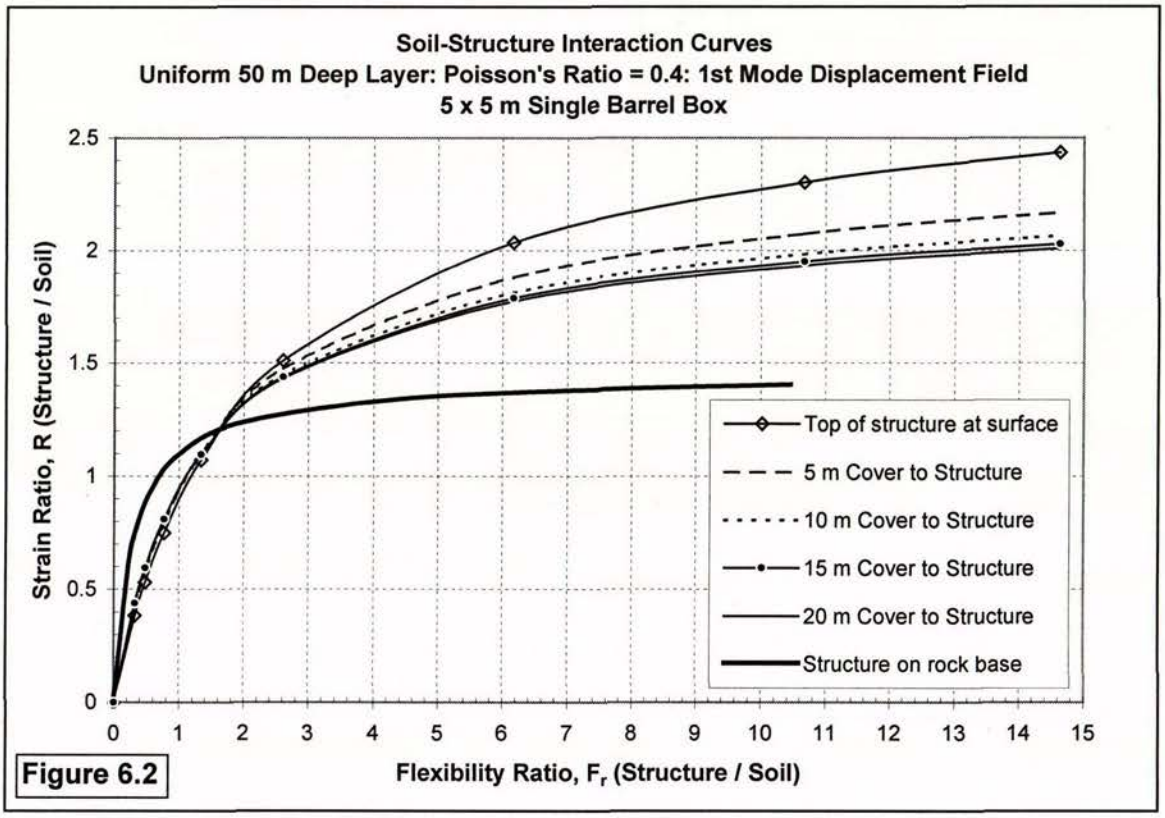

Figure 6.2

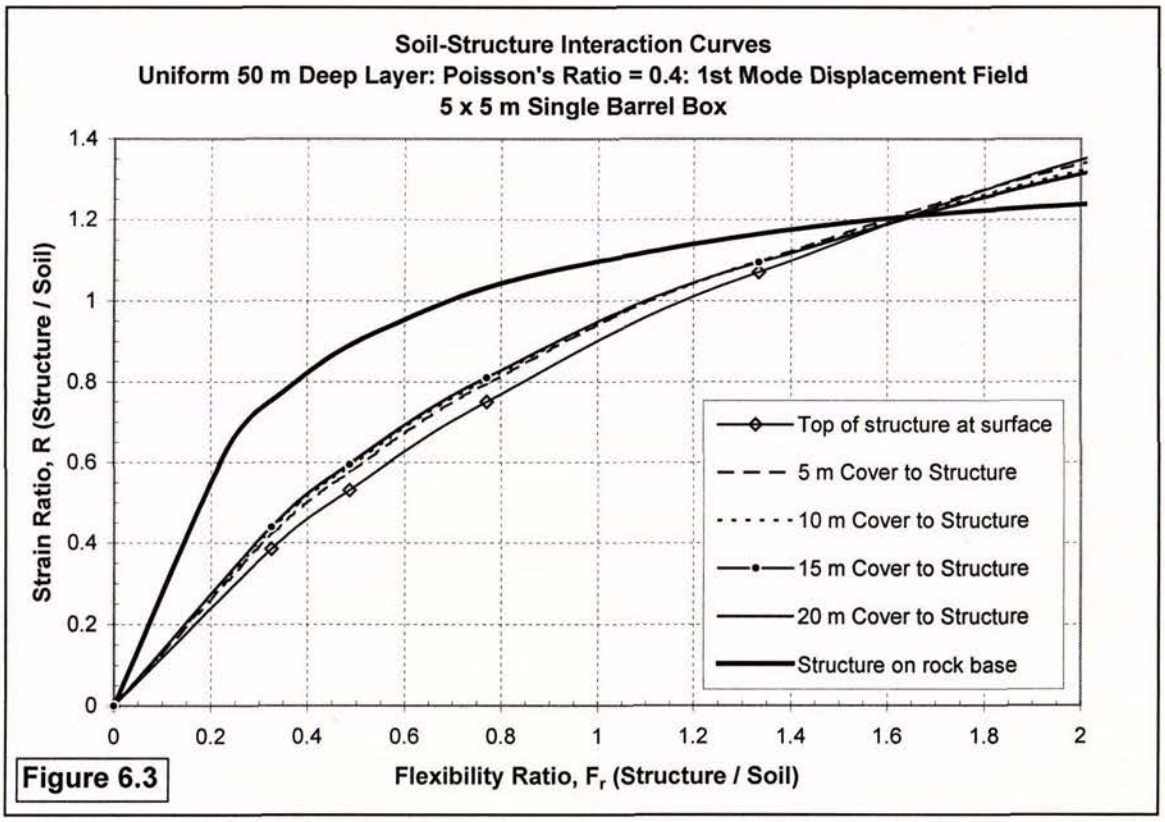

Figure 6.3

6.3 Influence of Layer Depth

R versus F_r curves for the single-barrel structure in a uniform 20 m thick layer are shown in Figures 6.4 and 6.5. Figure 6.4 shows the F_r ratio out to the maximum value investigated of 15 and Figure 6.5 the curves with an expanded scale for F_r from 0 to 2.0.

A comparison between the interaction curves for the 20 and 50 m deep layers is shown in Figure 6.6. As indicated by this plot, the depth of the layer has little influence on the interaction except when the structure is close to or supported on the rigid base. Because the structure height of 5 m is significant in relation to the 20 m depth of the shallower layer, the rigid base effect causes some differences in the higher F_r part of the curves. Layers significantly deeper than 20 m would give similar results to the 50 m deep layer for the case when the structure is founded on the rigid base or in the layer close to the base.

6.4 Influence of Strain Field

R versus F_r curves for the single-barrel structure in the 50 m thick layer with a parabolic increase of the shear modulus, G, with depth are shown in Figures 6.7 and 6.8. Figure 6.7 shows the F_r ratio out to the maximum value investigated of 15 and Figure 6.8 the curves with an expanded scale for F_r from 0 to 2.0.

A comparison between the interaction curves for 50 m deep layers with uniform and parabolic variation of G with depth are shown in Figure 6.9. Provided the depth of cover is greater than the height of the structure the variation in the shear modulus or strain field has little influence on the interaction. With shallow cover depths less than the height of the structure there are significant differences in the interaction curves. This is apparently caused by the large variation of the G value from zero at the surface to a moderately high value at the base of the structure that occurs in the layer with the parabolic variation. The low G values near the surface cause the structure to be effectively stiffer with respect to the soil than is the case for the structure in a uniform layer. For the purpose of plotting the curves, the effective G value was taken as the average over the height of the structure. Defining the effective G value as either the value at the top or base of the structure would obviously modify the curves for the structure in a layer with a parabolic G variation, particularly when the structure is near the surface.

6.5 Influence of Structure Shape

R versus F_r curves for the twin-barrel structure in 50 m thick layers with both a uniform and a parabolic increase of the shear modulus, G, with depth are shown in Figures 6.10 and 6.11. Figure 6.10 shows the F_r ratio out to the maximum value investigated of 15 and Figure 6.11 the curves with an expanded scale for F_r from 0 to 2.0.

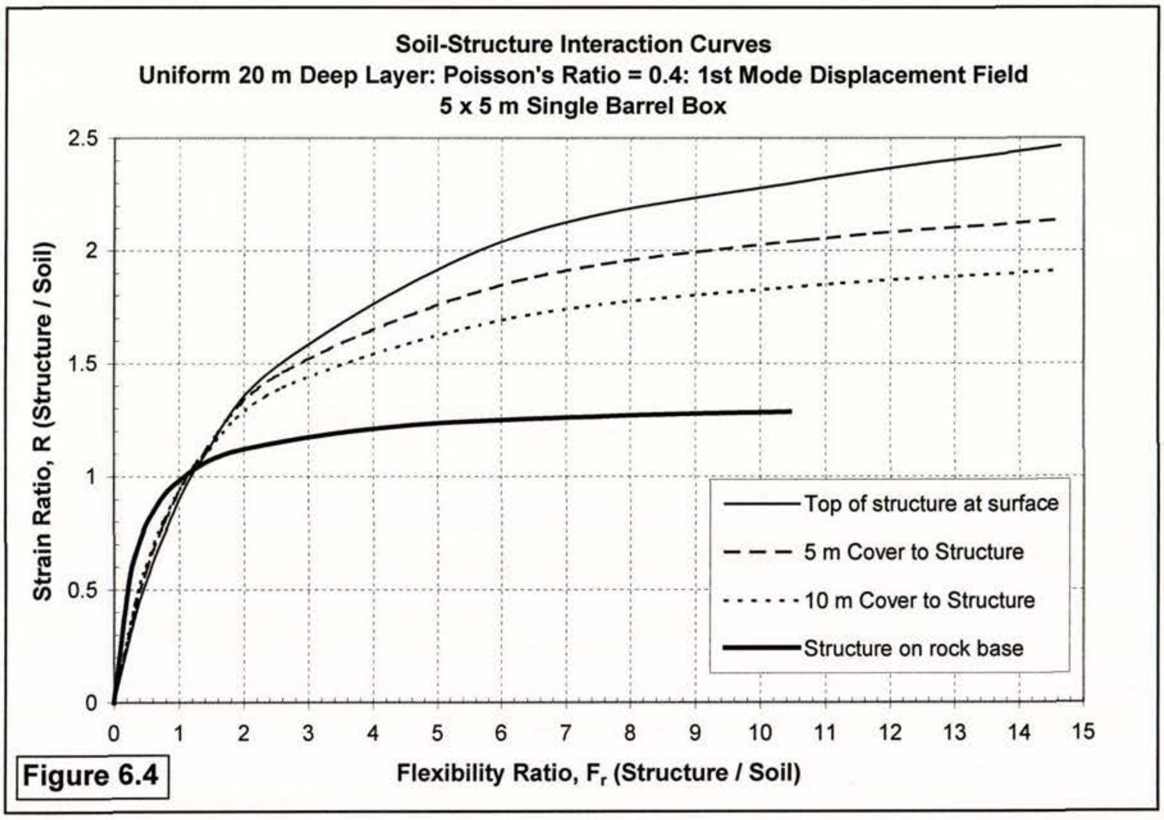

Figure 6.4

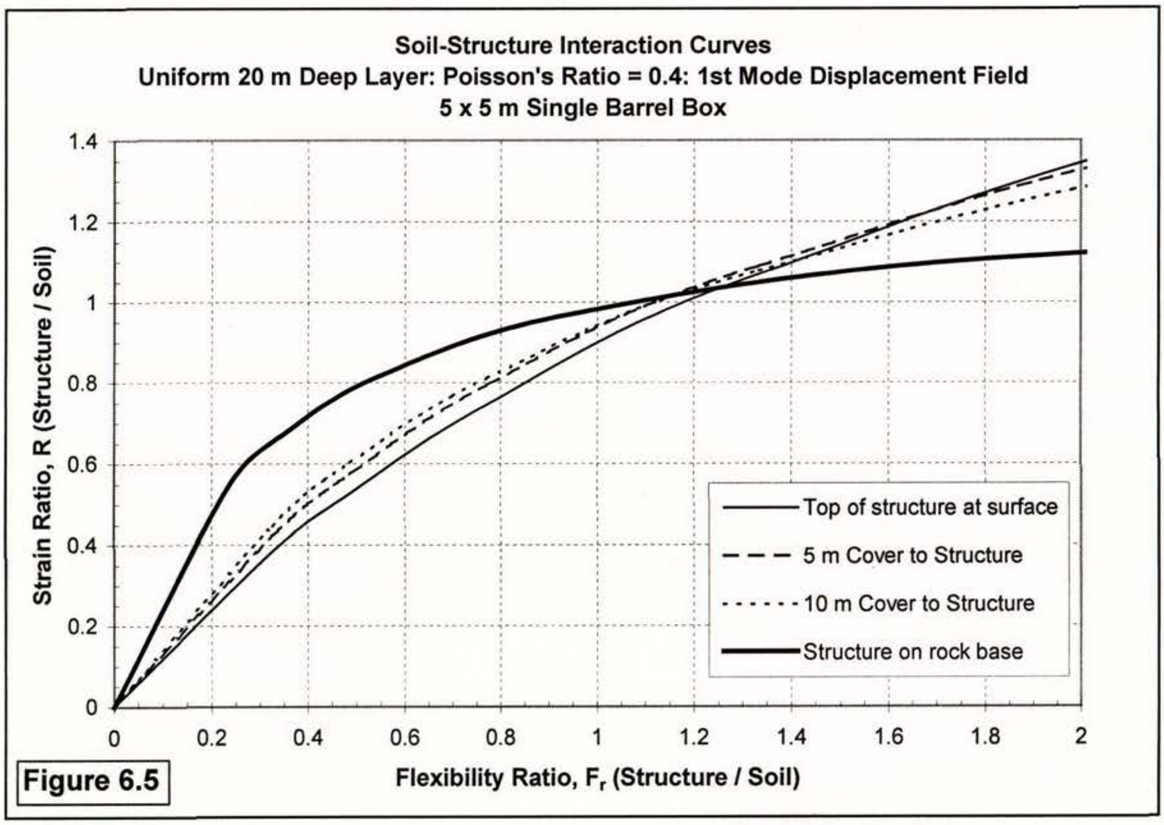

Figure 6.5

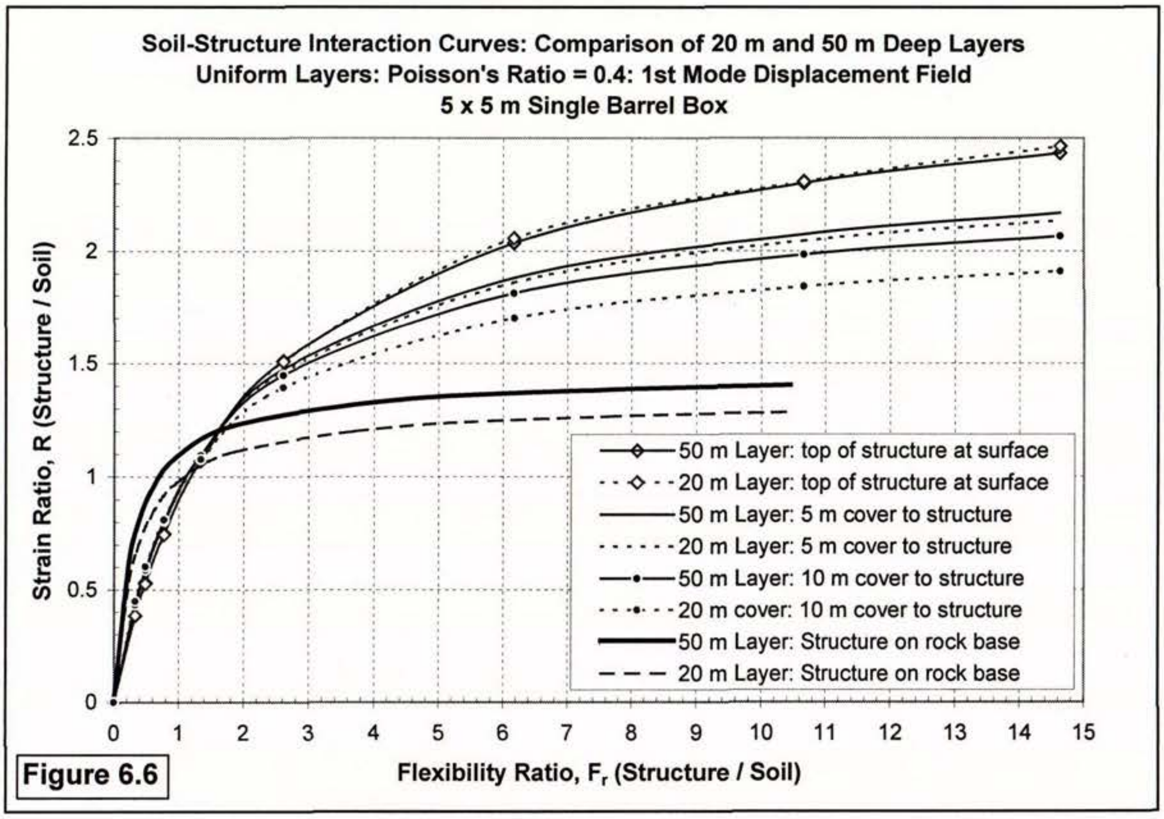
Soil-Structure Interaction Curves: Comparison of 20 m and 50 m Deep Layers
Uniform Layers: Poisson's Ratio = 0.4: 1st Mode Displacement Field
5 x 5 m Single Barrel Box
Strain Ratio, R (Structure / Soil)
Flexibility Ratio, Fr (Structure / Soil)
50 m Layer: top of structure at surface
20 m Layer: top of structure at surface
50 m Layer: 5 m cover to structure
20 m Layer: 5 m cover to structure
50 m Layer: 10 m cover to structure
20 m cover: 10 m cover to structure
50 m Layer: Structure on rock base
20 m Layer: Structure on rock base

Figure 6.6

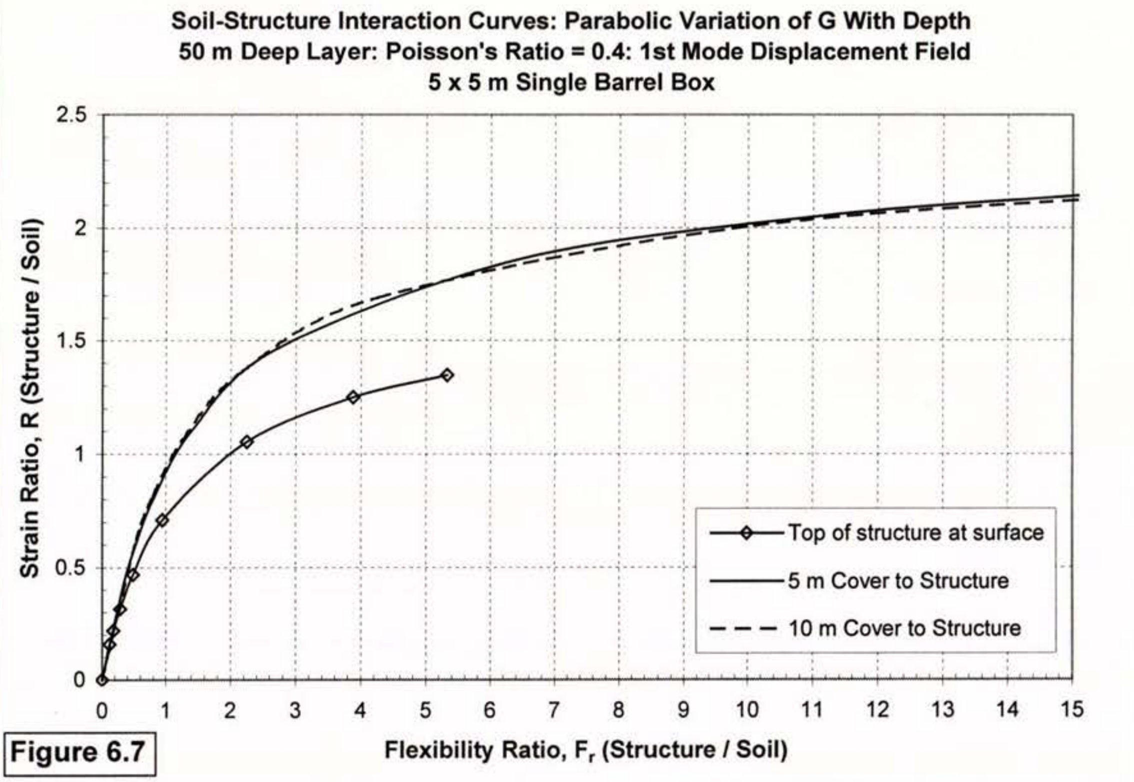

Figure 6.7

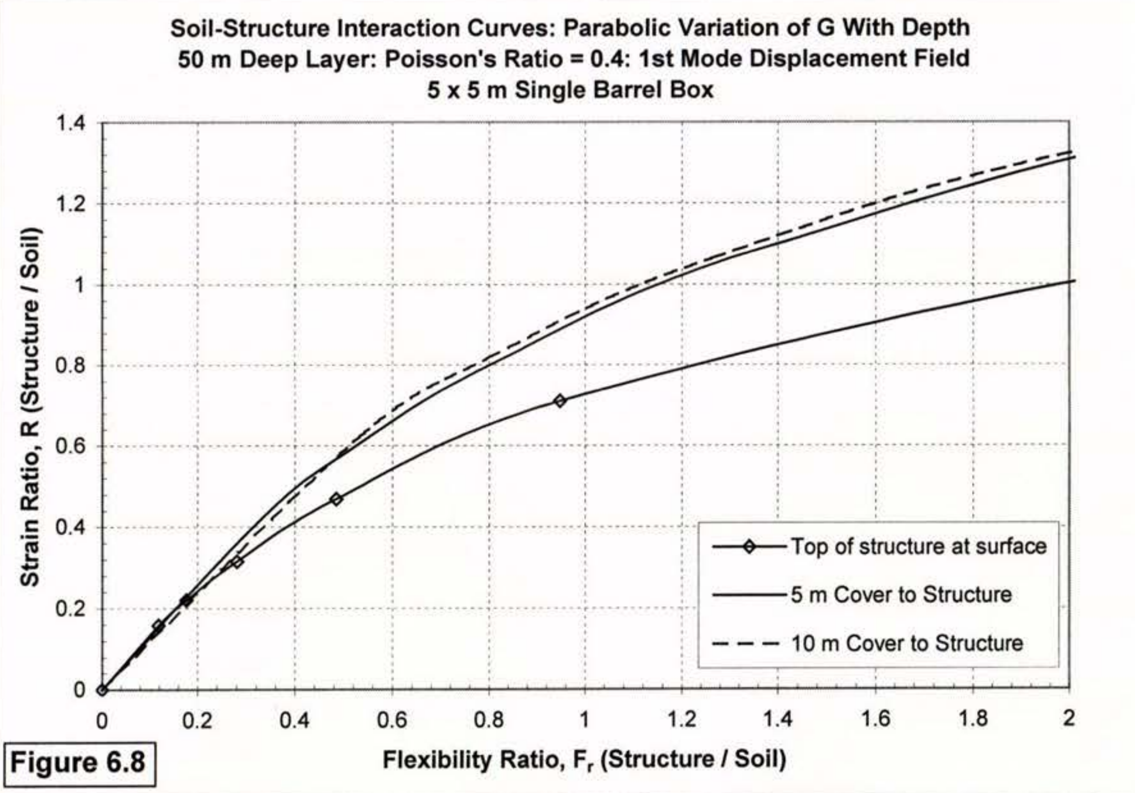

Figure 6.8

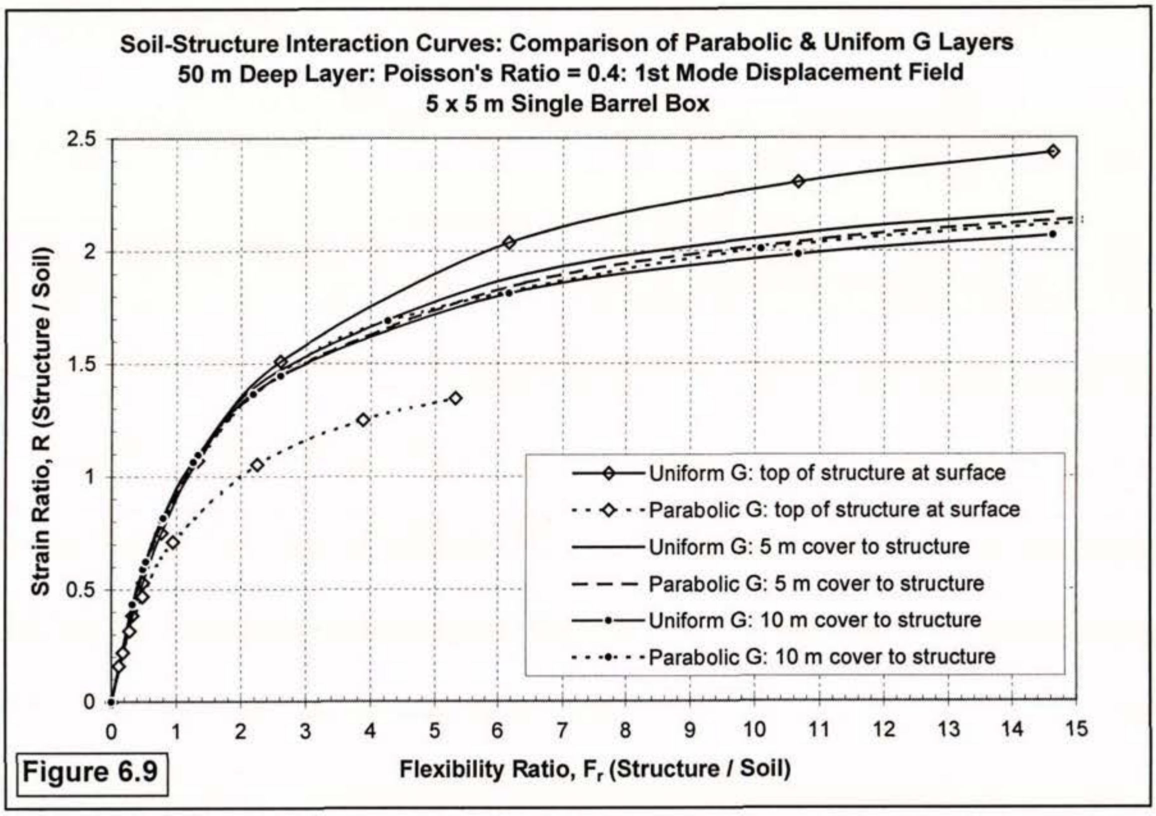

Soil-Structure Interaction Curves: Comparison of Parabolic & Unifom G Layers
50 m Deep Layer: Poisson's Ratio = 0.4: 1st Mode Displacement Field
5 x 5 m Single Barrel Box
Strain Ratio, R (Structure / Soil)
Flexibility Ratio, F$_r$ (Structure / Soil)
0
0.5
1
1.5
2
2.5
0 1 2 3 4 5 6 7 8 9 10 11 12 13 14 15
Uniform G: top of structure at surface
Parabolic G: top of structure at surface
Uniform G: 5 m cover to structure
Parabolic G: 5 m cover to structure
Uniform G: 10 m cover to structure
Parabolic G: 10 m cover to structure

Figure 6.9

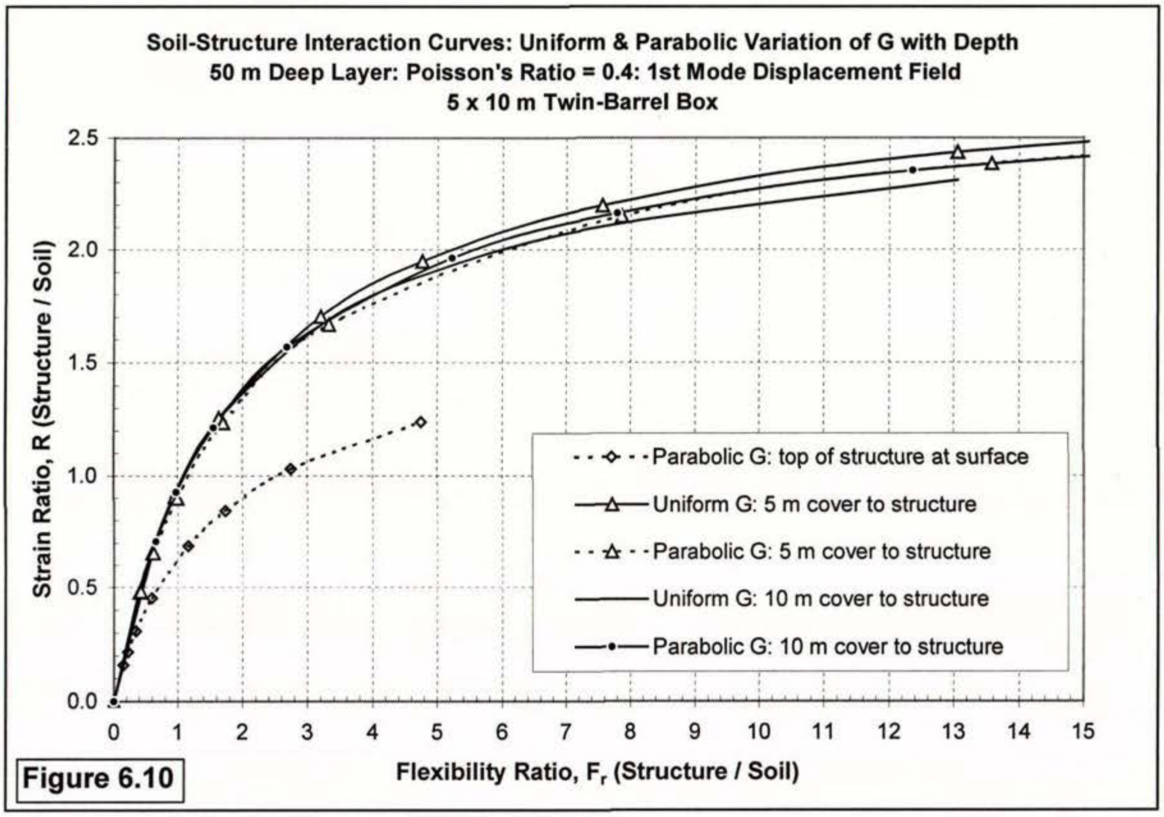

Figure 6.10

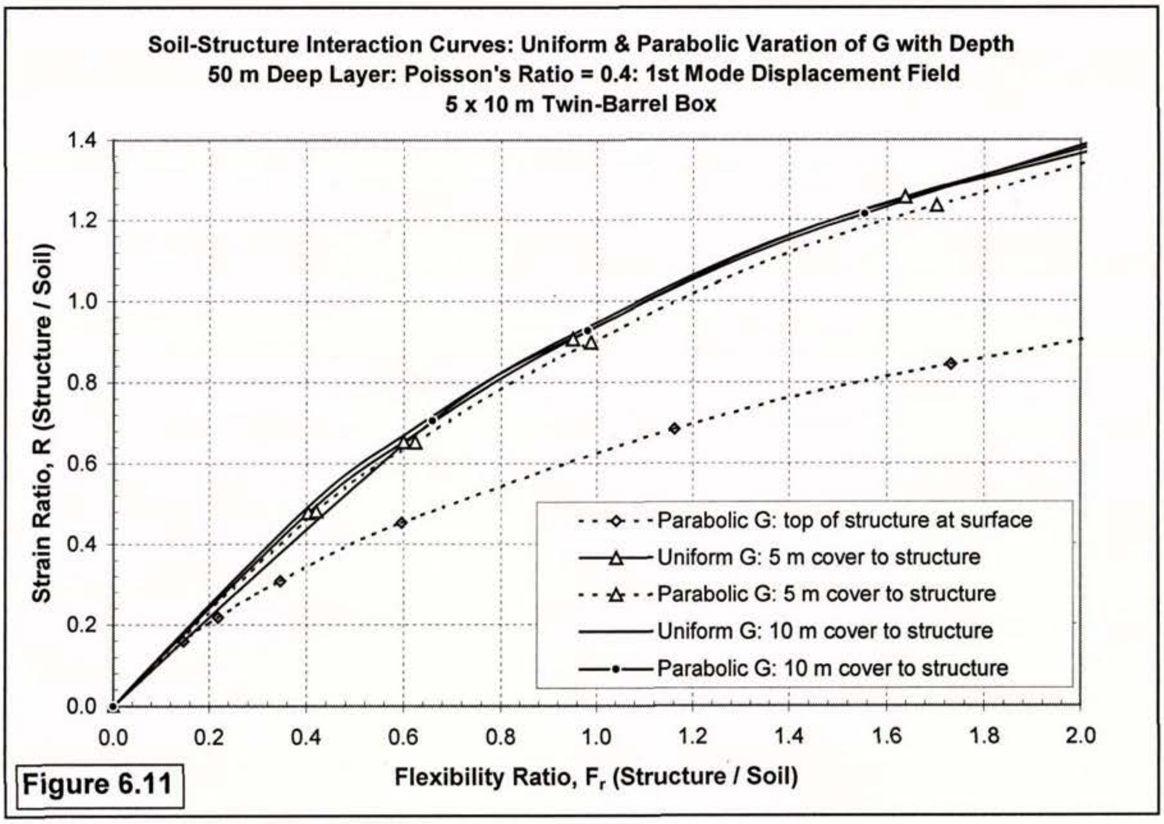

Figure 6.11

A comparison between the interaction curves for the single and twin-barrel structures is shown in Figure 6.12 and 13 for cover depths of 5 and 10 m respectively. For F_r ratios less than 2.0 the structure shape has little influence, however at greater F_r ratio the shape causes a moderate degree of divergence of the curves.

6.6 Influence of Soil Poisson's Ratio

Further work to estimate the influence of soil layer Poisson's Ratio on the interaction curves using the finite element procedure of the present study is planned but until this is completed the Poisson Ratio effect can be estimated approximately by Penzien's analytical expression.

R versus F_r curves evaluated using Equation 6.14 for a range of Poisson's Ratio from 0.3 to 0.5 are shown in Figure 6.14. Poisson's ratio has a moderately significant influence on the interaction curves when F_r is greater than 2.0, particularly for Poisson's ratio less than 0.4.

6.7 Forces in Box Structural Members Without Soil Interaction

Simple structural analysis, such as the Slope Deflection Method, can be used to analyse the laterally loaded single-barrel box shown in Figure 5.4 without surrounding soil to give the bending moments, shear and axial forces in the members. Expressions for the bending moments M_r and M_f acting in the members at the top and bottom rigid joints respectively in terms of the lateral displacement Δ are:

$$M_f = \frac{6\Delta K_w}{H}\left[\frac{j(3+q)}{(j-(2j+q)(2+q)}\right] \tag{6.1}$$

$$M_r = \frac{6\Delta K_w}{H}\left[\frac{j(3+q)(2+q)}{(j-(2j+q)(2+q)}+1\right] \tag{6.2}$$

Where:

$$K_w = \frac{EI_w}{H} \qquad K_r = \frac{EI_r}{H} \qquad q = \frac{K_w}{K_r}$$

The shear and axial forces in the wall members are obtained from the equilibrium equations to be $\frac{P}{2}$ and $\frac{PH}{2L}$ respectively.

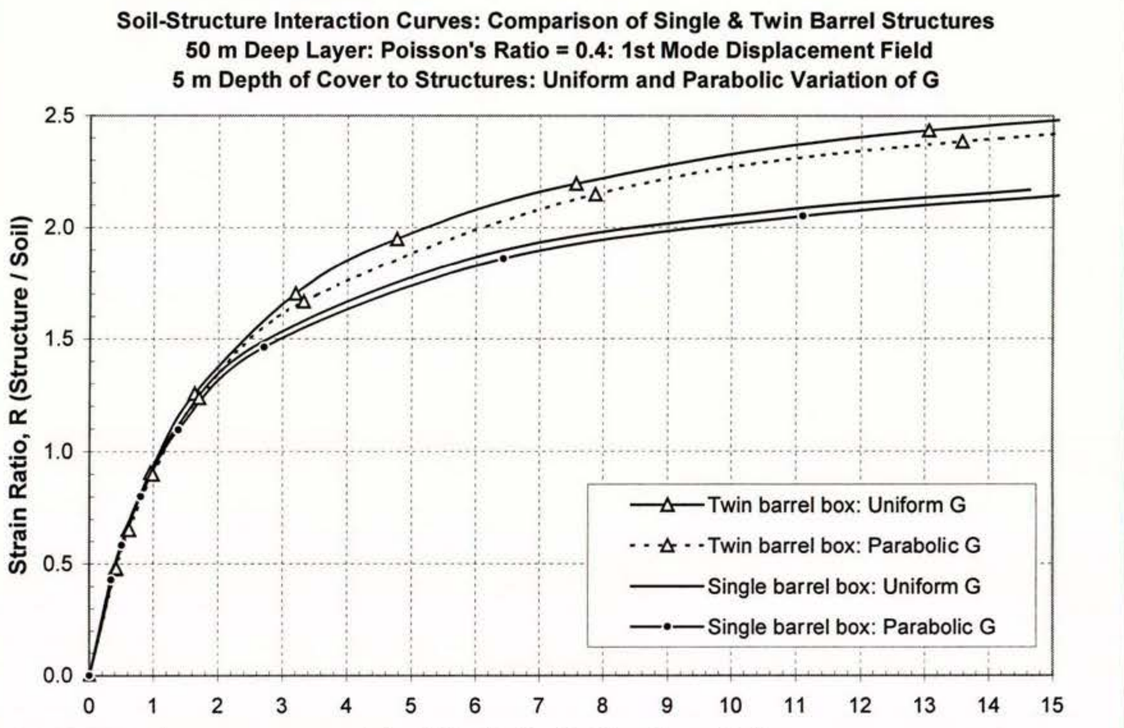

Figure 6.12

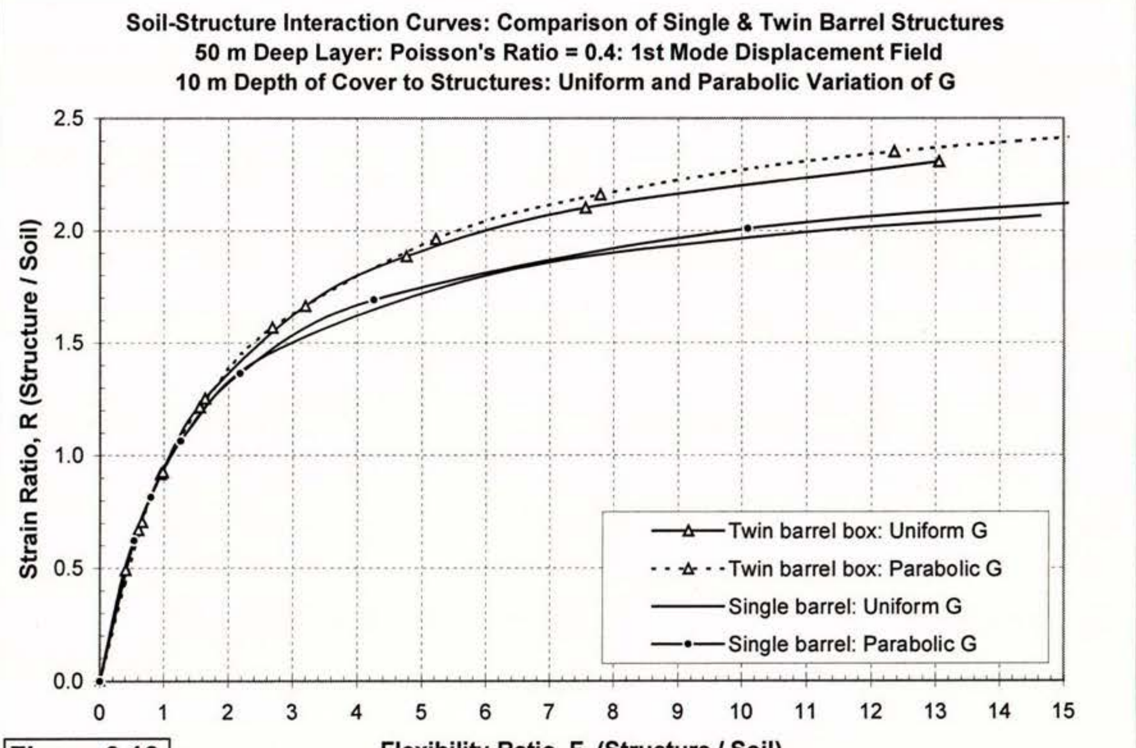

Figure 6.13

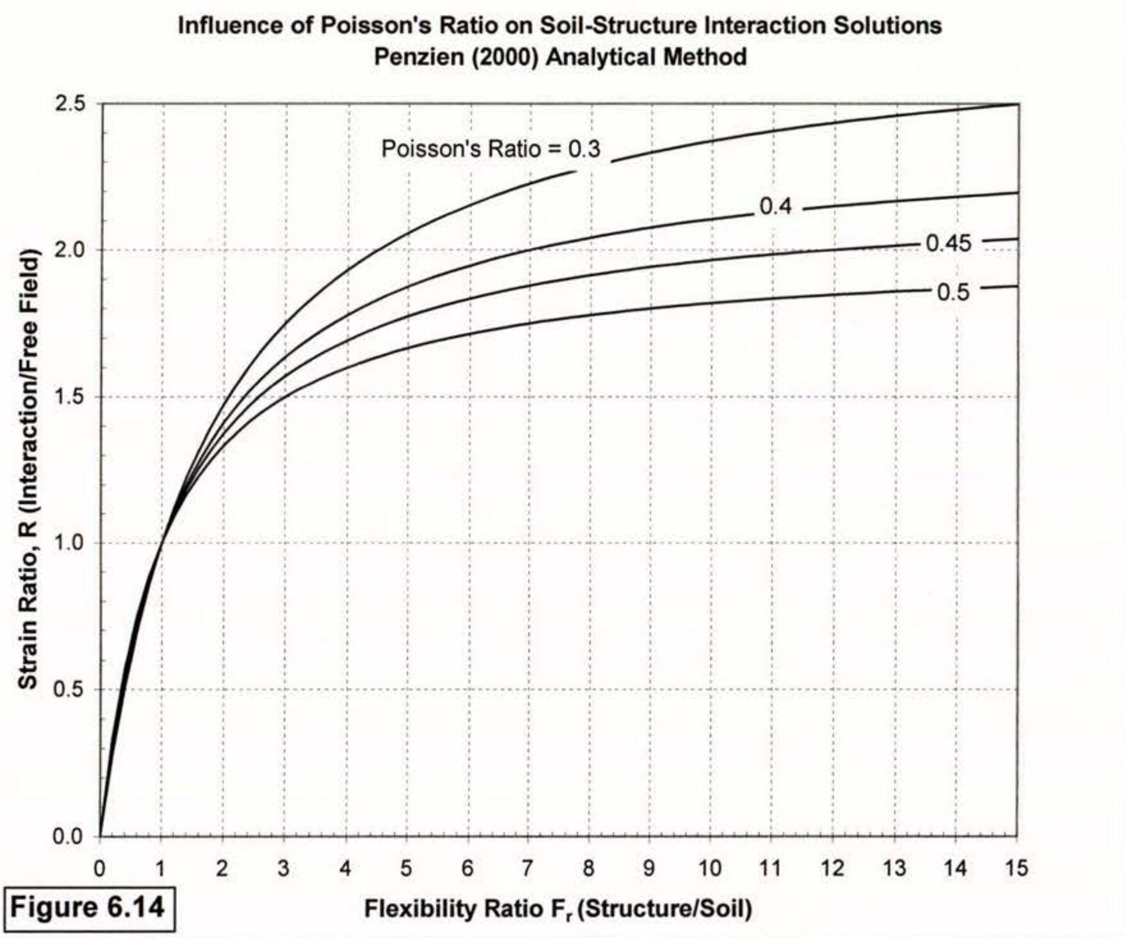

Influence of Poisson's Ratio on Soil-Structure Interaction Solutions
Penzien (2000) Analytical Method
Poisson's Ratio = 0.3
0.4
0.45
0.5
Strain Ratio, R (Interaction/Free Field)
2.5
2.0
1.5
1.0
0.5
0.0
0 1 2 3 4 5 6 7 8 9 10 11 12 13 14 15
Flexibility Ratio F_r (Structure/Soil)

Figure 6.14

6.8 Forces in Box Structural Members With Soil Interaction

Forces in the structural members of the single and twin-barrel box structures analysed in the interaction analyses described in Section 5.3.4 were calculated by the finite element procedure.

The bending moments and shear forces in the side-wall members computed for the single and twin-barrel box structures with a 5 m depth of cover are shown in Figures 6.15 to 6.18. Results are given for both a uniform and parabolic variation of G in a layer of 50 m depth. Figures 6.15 and 6.16 show the bending moments at the top and bottom of the side-walls respectively and Figures 6.17 and 6.18 the corresponding shear forces.

Figures 6.19 to 6.22 show results corresponding to those shown in Figures 6.15 to 6.18 but with the depth of cover increased from 5 m to 10 m.

Both the plotted interaction bending moments and shear forces have been normalised by dividing the computed values by the corresponding values for the structures without surrounding soil. For the single-barrel structures, Equations 6.1 and 6.2 were used to compute the side-wall bending moments for the case without surrounding soil. For the twin-barrel structures, a simple plane frame computer analysis was used to calculate the moments for this case. (Closed form analytical solutions can be developed but it was less time consuming to use a numerical method.) In interpreting the results, it is important to note that the analyses without the surrounding soil require the structure to be supported by pinned reaction points under the lower corners which prevent vertical displacements (see Figure 5.4). This imposes different boundary conditions than occur when the structure is supported only by the surrounding soil. In the later case, the structure can undergo rigid body rotations, which may influence the magnitude of the internal forces in the structural members. For this reason, not all the plotted moments and shears tend to a value of 1.0 as the flexibility ratio, or effectively the soil stiffness, reduces to zero.

From the results plotted in Figures 6.15 to 6.22 it is apparent that the interaction effects significantly modify the bending moments and shear forces in the box members for large F_r ratios. Previous recommendations (Wang, 1993) have suggested that the forces in the box structure can be obtained by analysing the structure without the soil loaded by a horizontal force at the top that produces the same shear distortion as calculated from the shear strain interaction analysis. However, the present analyses show that for values of F_r greater than 1.0, the force actions cannot be reliably obtained by this procedure. Better approaches would be to use a simple finite element analysis including the soil (the method outlined in this project for example) or the curves shown in Figures 6.15 to 6.22 to correct the actions computed by a frame analysis without the soil.

To calculate the flexural strength capacities of the box section walls it is also necessary to know the axial forces in them. Information on these actions is available from the present work and will be presented at a later time. The variation of the normalised axial forces with F_r ratio will be similar to that shown for the normalised bending moments.

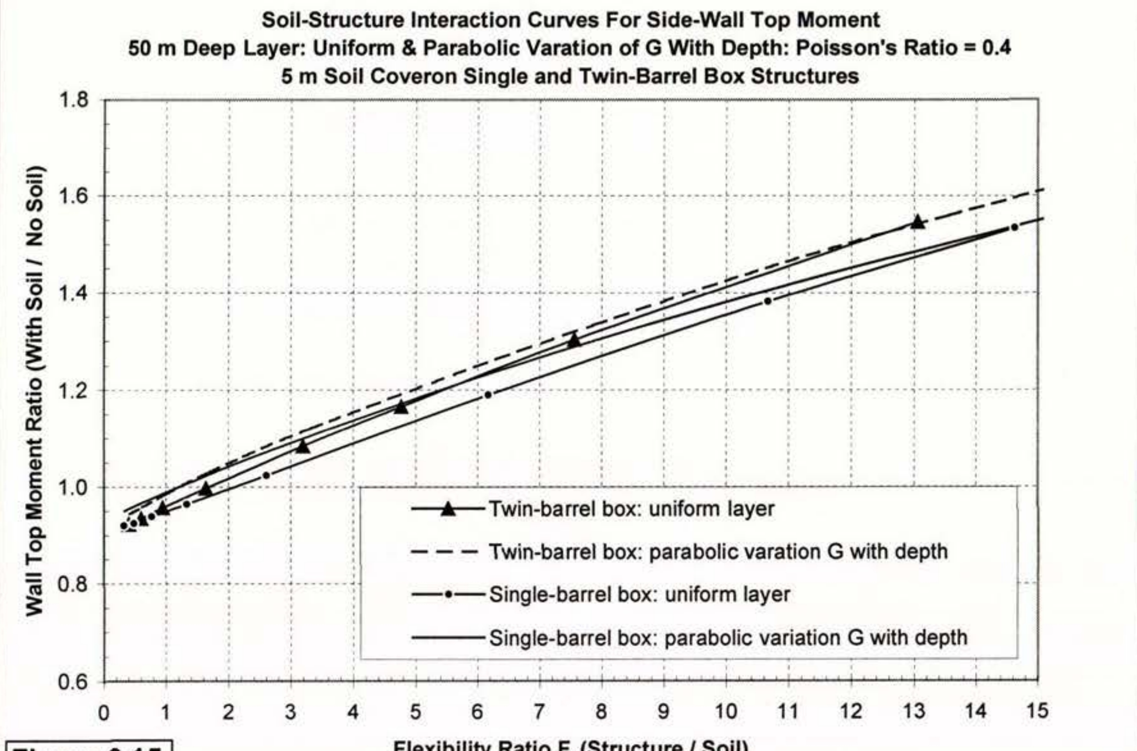

Figure 6.15

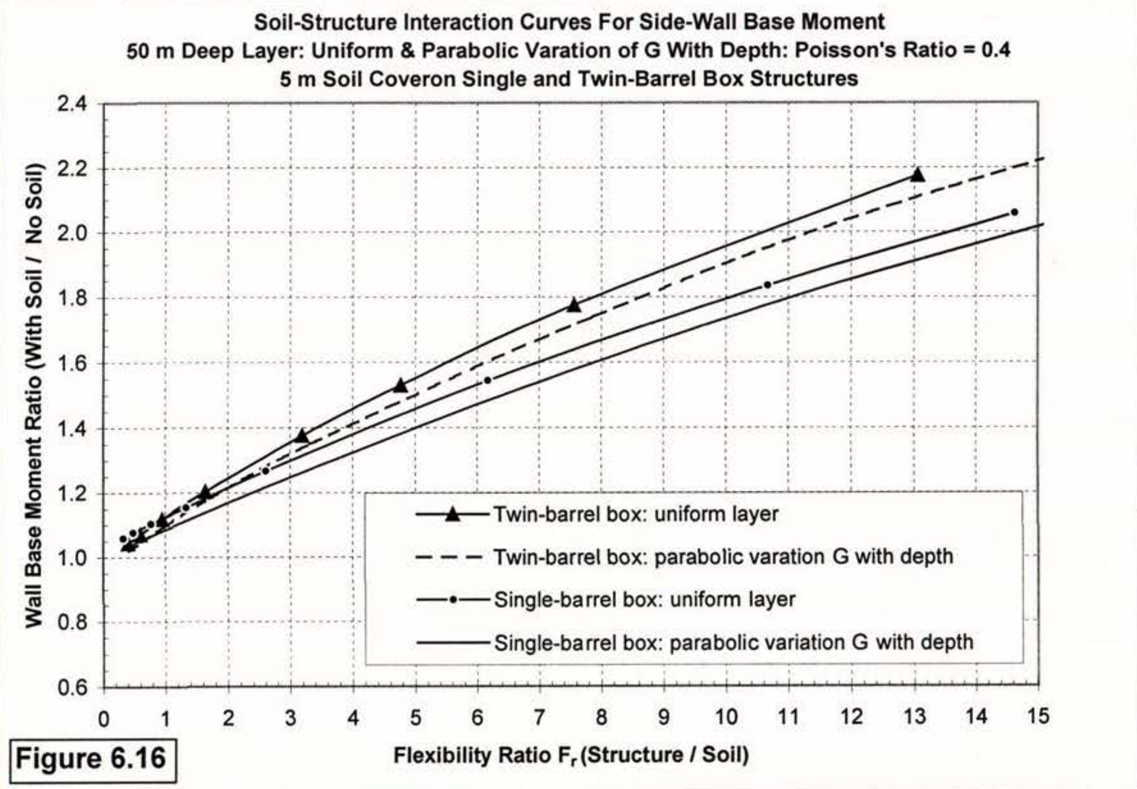

Figure 6.16

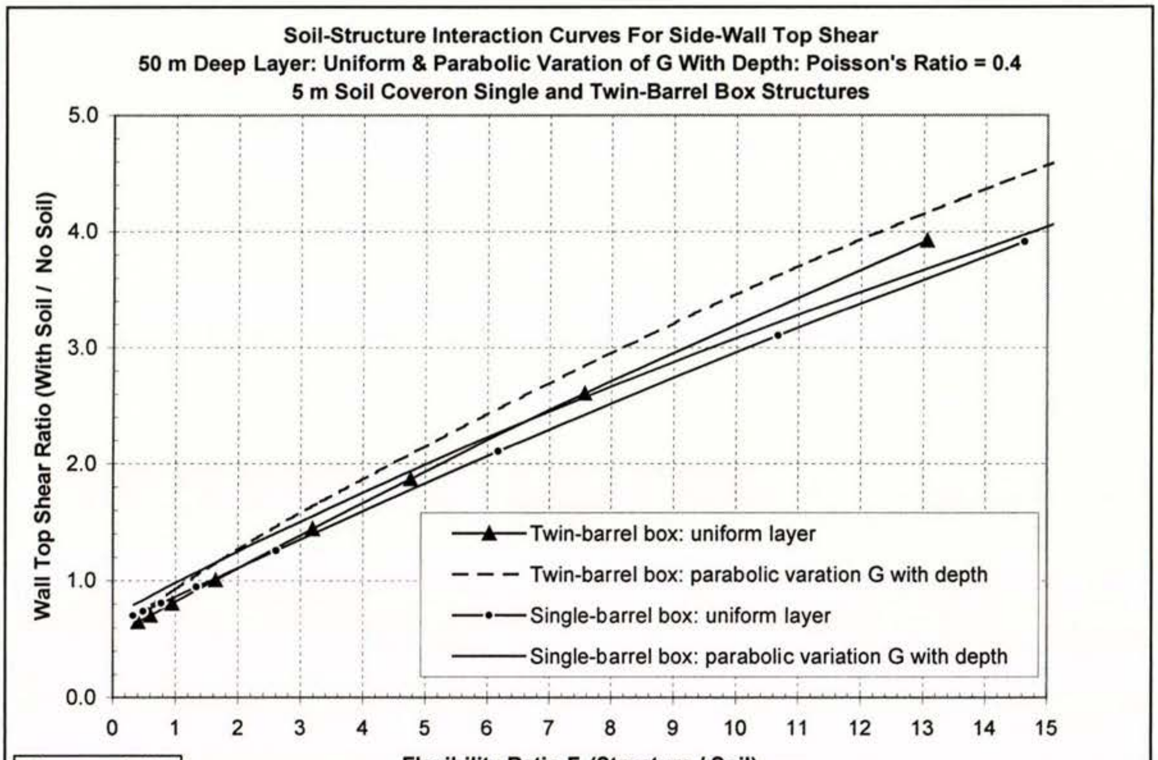

Figure 6.17

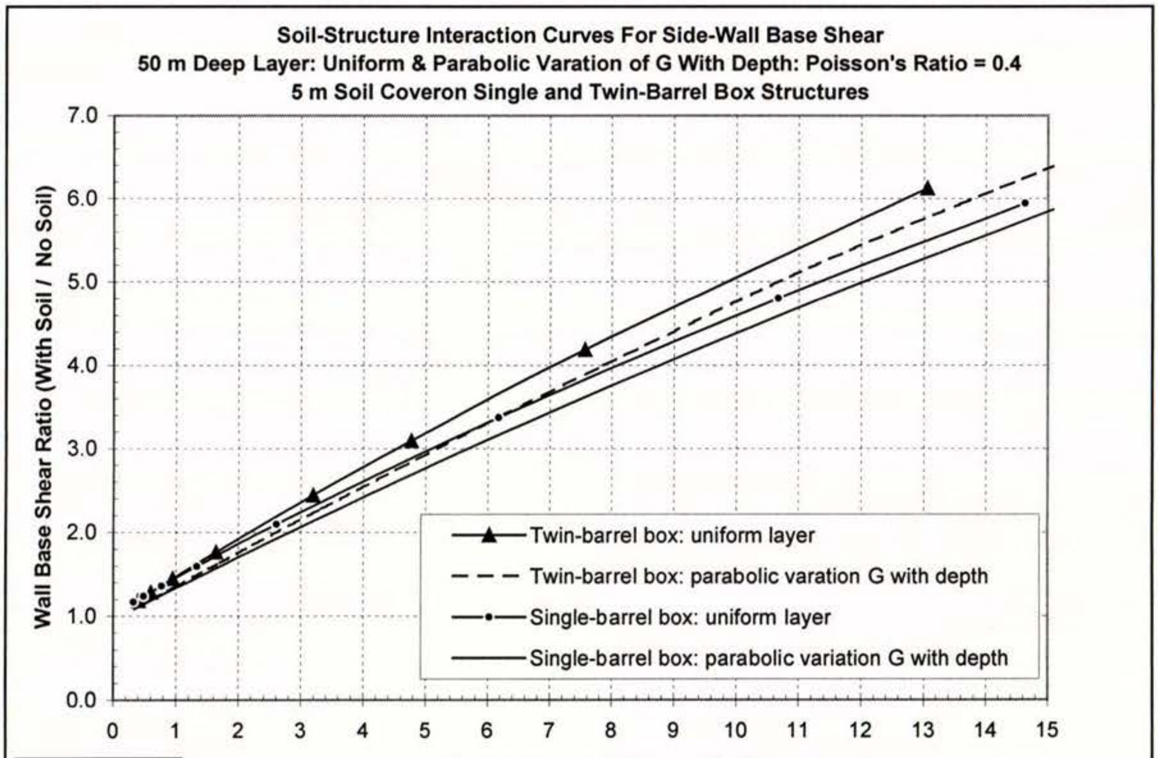

Figure 6.18

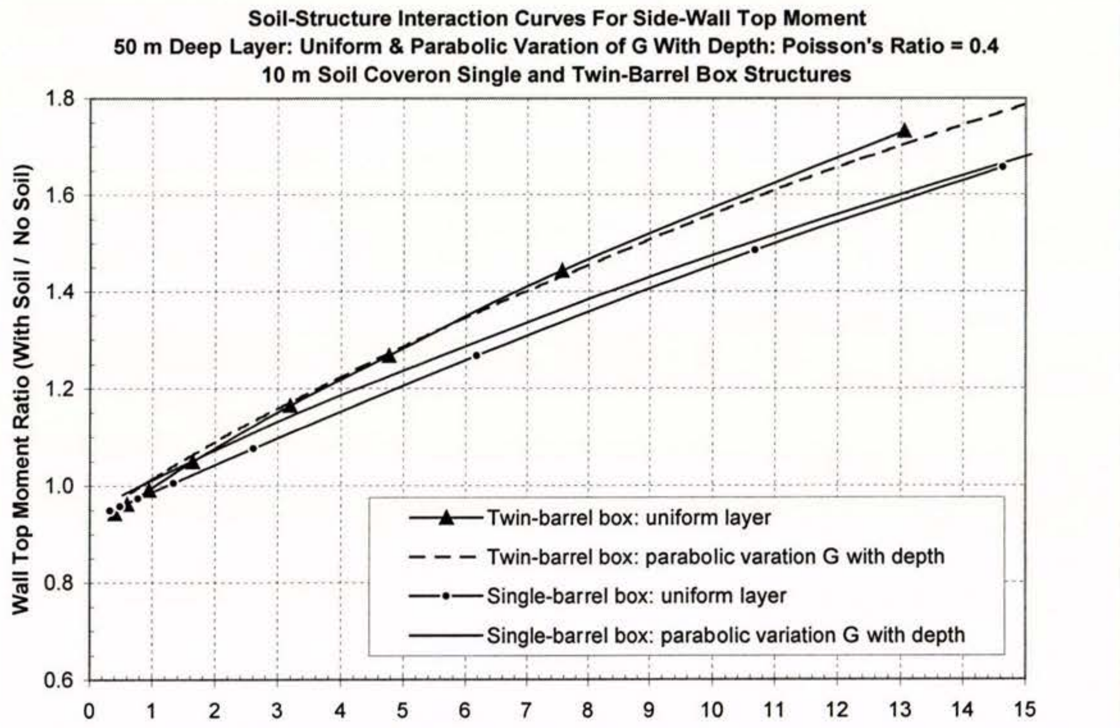

Figure 6.19

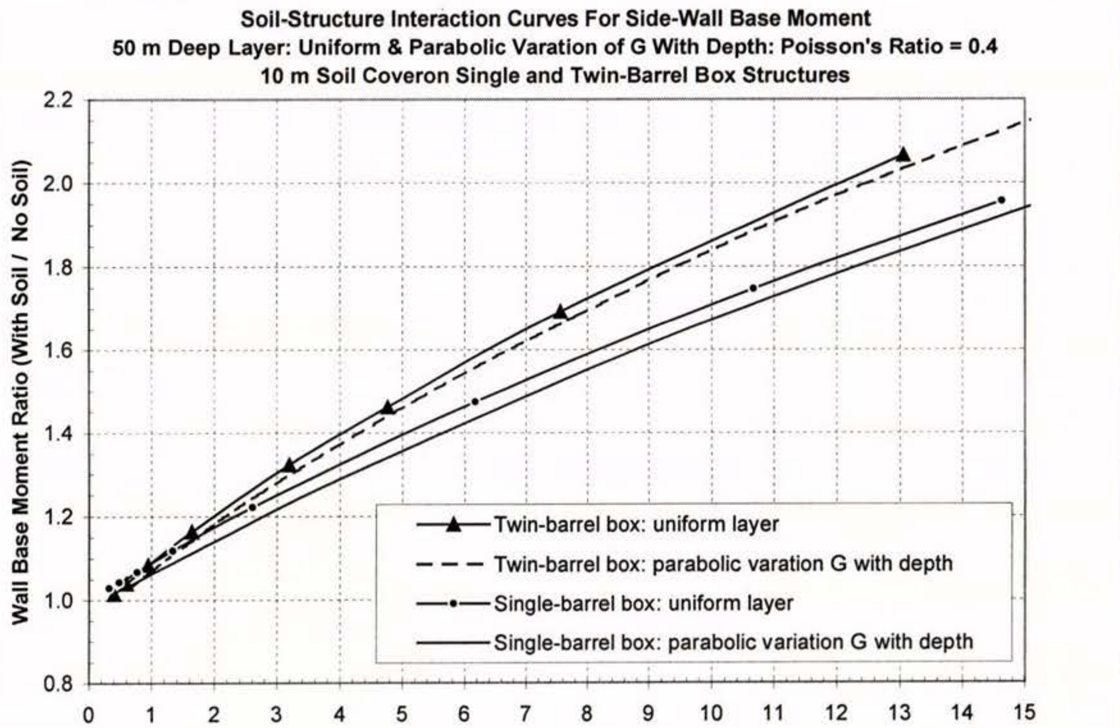

Figure 6.20

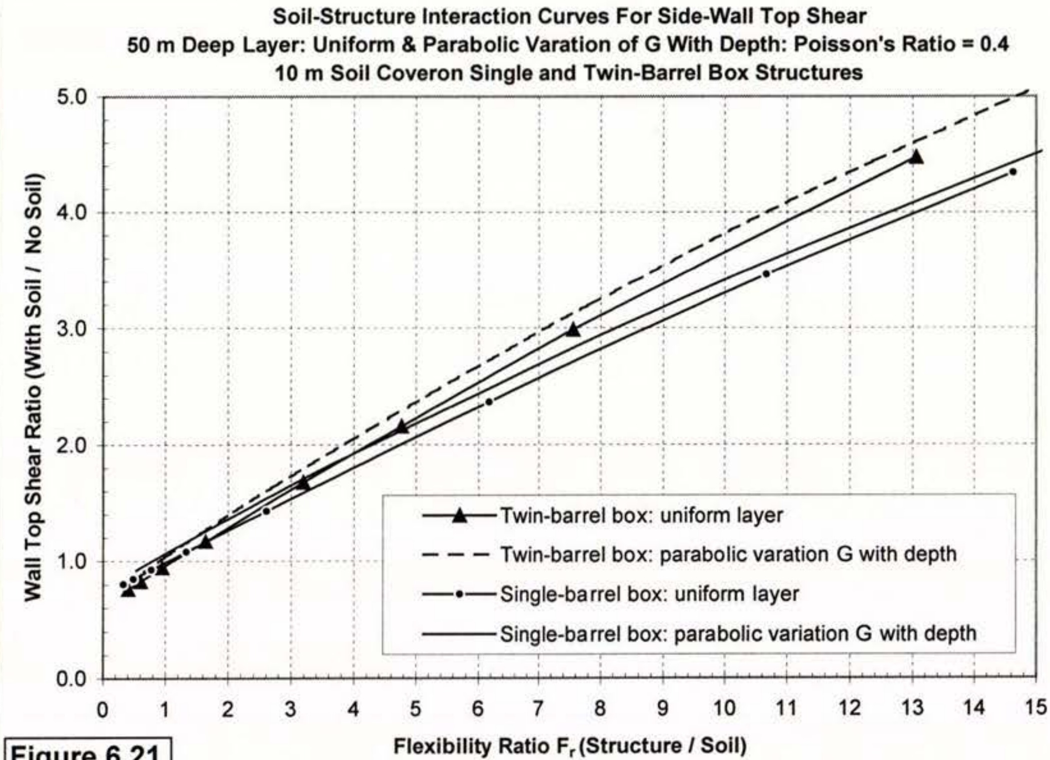

Figure 6.21

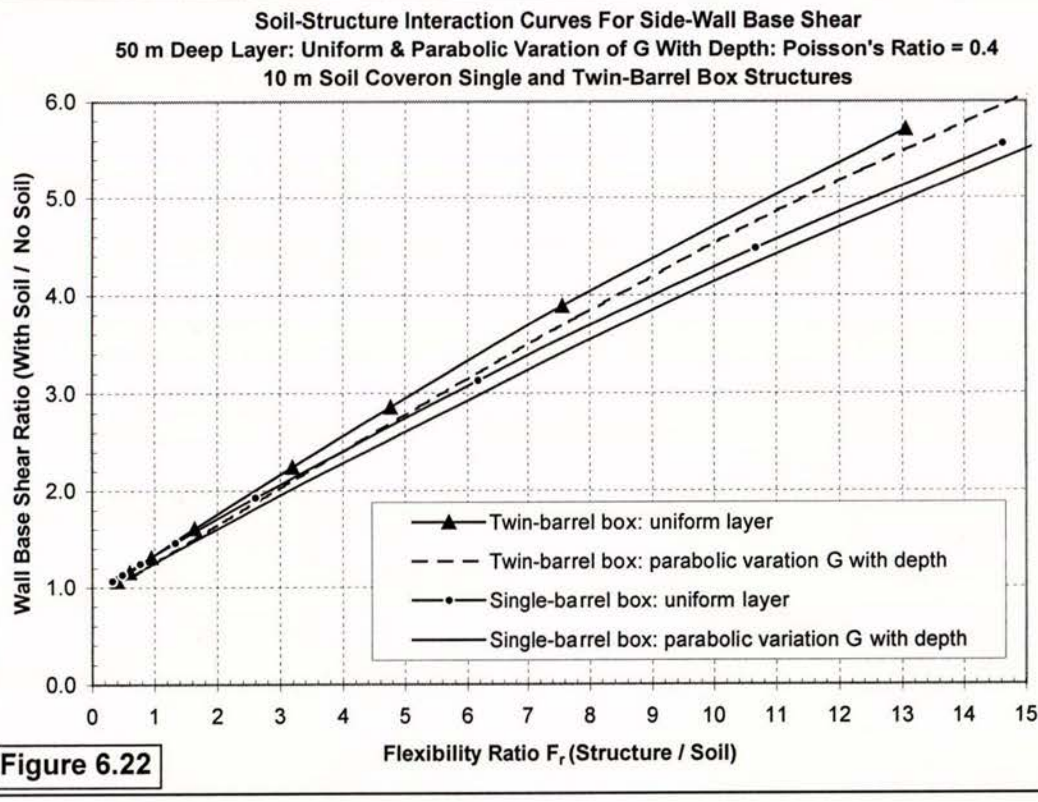

Figure 6.22

7. WORKED EXAMPLES

The application of the methods and results developed in this study is illustrated in the following sections by analysing two examples of relatively small and commonly constructed underground structures. The first example is a single-barrel box culvert structure originally designed by the New Zealand Ministry of Works and Development in 1976. It was one of a number standard culvert designs (see MWD drawings Job 0/121/1 Code 8104) and similar structures to the one analysed have probably been constructed in a number of locations in New Zealand. The structure used in the second example is a similar structure to the first example but the wall thicknesses and reinforcement quantities have been reduced to make the structure more typical of a pedestrian subway structure constructed in dry ground conditions without water pressures. The structure analysed in the first example was found to respond essentially elastically under typical design earthquake ground acceleration levels. The second structure was found to respond into its inelastic range of behaviour with plastic hinges forming at the corner rigid joints.

7.1 Box Culvert Example

Details of the structure analysed are given in Figure 7.1 and Table 7.1. The standard culvert box structure has internal dimensions of 3 x 3 m and was assumed to be covered by 4 m of soil in a 50 m deep soil layer with a shear modulus G varying parabolicaly from zero at the surface to 200 MPa at the rigid base. The average calculated G value over the height of the structure was 44 MPa corresponding to a shear wave velocity of about 150 m/s. This velocity indicates medium density sediments. The design peak ground acceleration at the surface was taken as 0.4 g.

The walls were assumed to have a uniform thickness of 400 mm although in practise most culverts are constructed with a 50 mm thicker base to allow for water erosion. Reinforcement details for the side-walls are listed in Table 7.1. The same details apply to the outside bars in the roof and floor. Bars on the inside of the roof and floor are D28 at 250 mm centres.

The analysis procedure follows through sequentially on the spreadsheet of Table 7.1. A summary of the steps involved is as follows:

(a) Calculate the average shear modulus over the height of the structure.

(b) Calculate the structure stiffness and flexibility parameters using the formulae given in Section 5.2. Modify the stiffness parameters to allow for cracking in the box sections if necessary.

(c) Calculate the Fr and R ratios using the equations given in Section 5.3. (Penzien's Equation 5.10 was adopted to calculate R for his example but the charts in Figures 6.2 to 6.13 can be used to get more correct values.)

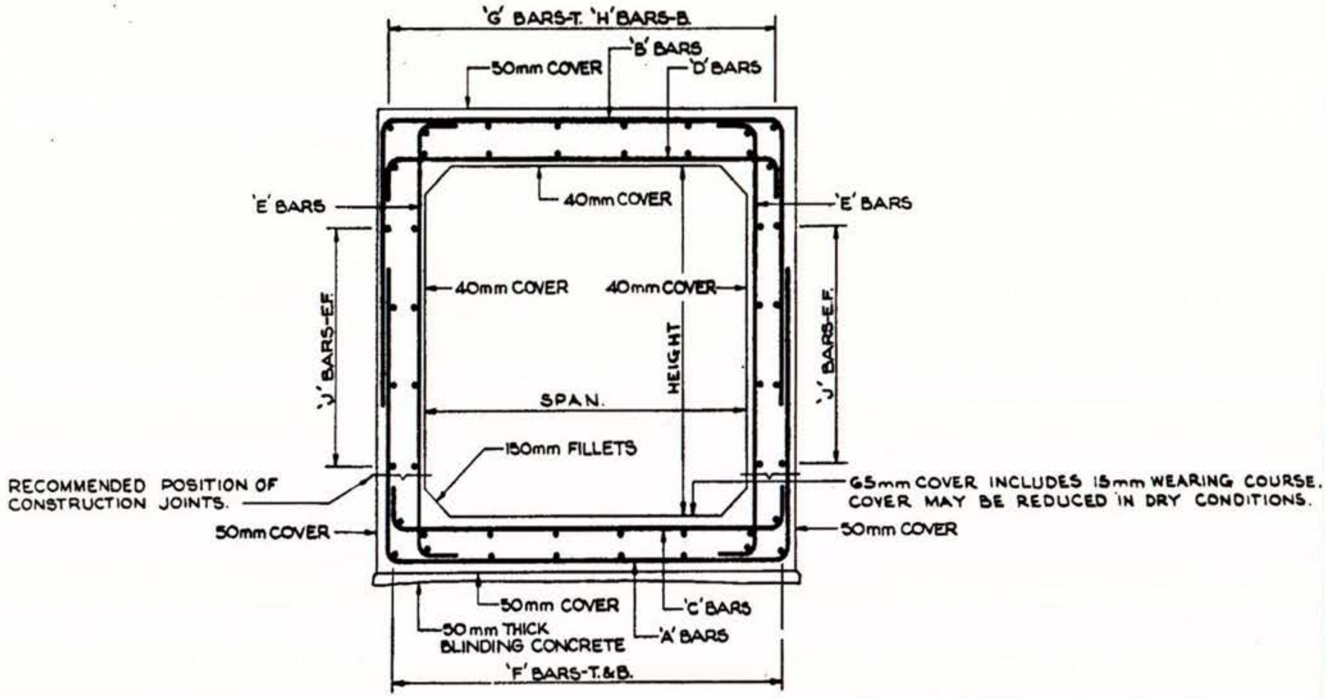

Figure 7.1 Standard box culvert structure analysed in Example 1 (Source MWD 1976).

(d) Calculate the design earthquake level surface strain and the soil strain at the level of the structure using Figure 5.3 and correct for the soil layer base shear modulus using Equation 5.3. (G_b assumed to be 200 MPa, which is different to the chart value of 150 MPa.)

(e) Calculate the structure shear deflection from the interaction shear strain and then calculate the earthquake induced moments in the structure using Equations 6.1 and 6.2.

(f) Correct the calculated bending moments for soil pressure effects using Figure 6.19 and 6.20.

(g) Calculate the flexural strength capacities of the box sections.

(h) Calculate the gravity load bending moments using a standard frame analysis procedure. (For simplicity in the present example water pressures have been neglected but where the produce significant loads they can be combined with the gravity load actions).

(i) Combine the earthquake and gravity load moments. The resulting bending moment diagram for the present example is shown in Figure 7.2

(j) Compare the combined E + G bending moments with the section capacities. From this comparison it is clear that a plastic hinge will form at the bottom left corner of the box. (Axial forces will enhance the flexural strengths slightly, particularly in the right wall in which the earthquake and gravity axial forces are additive.)

(k) From the earthquake and combined E + G bending moments calculate by simple scaling the structural shear displacement necessary to form the first hinge. This is considered to be the yield displacement.

(l) Compare the yield displacement with the displacement induced by the shear response of the soil. This gives an indication of whether significant nonlinear deformation is induced in the structure.

The analysis indicates that the structure is deformed to slightly beyond the structure yield displacement by the 0.4 g peak ground acceleration motions. Significant cracking and minor damage would occur under this level of ground shaking. Although the structure would have been designed for significant water pressures they have been neglected in the analysis. If water pressures moments were included the level of inelastic deformation would be significantly greater than calculated.

The Draft AS/NZ 1170.4 Loadings Code indicates that the design peak ground acceleration on Site Subsoil Class D soils (the period of vibration of the layer used in the present example would be greater than 0.6 seconds) for a 500 year return period event in the Wellington area should be about 0.49. To allow for the averaging reduction over a number of damaging peaks in the acceleration time history, it would be normal to design an important underground structure to about the 0.4 g acceleration level used in the above example.

Table 7.1 Single-Barrel Box Culvert Structure Example

Item	Symbol	Value	Units	Comments or Formula
Soil Input Parameters				
Soil layer depth	D	50	m	
Soil cover depth over structure	D_s	4.0	m	
Shear modulus at base of soil layer	G_b	200	MPa	Layer assumed to have parabolic varation of G
Soil density	ρ_s	2.0	t/m^3	
Soil Poisson's Ratio	ν	0.4		
Structure Geometric Inputs				
Outside height (overall)	H	3.8	m	
Outside length (overall)	L	3.8	m	
Floor thickness	t_f	0.40	m	
Roof thickness	t_r	0.40	m	
Wall thickness	t_w	0.40	m	
Concrete Section Inputs				
Young's modulus for concrete	E_c	30000	MPa	
Concrete crushing strength	f_c	25	MPa	
Reinforcement yield stress	f_y	300	MPa	
Cracked section MOI reduct. factor	F_{cs}	0.50		
Concrete cover to reinforcement	c_s	40	mm	
Outer reinforcement bar diameter	d_b	24	mm	
Outer reinforcement bar spacing	S_b	200	mm	
Inner reinforcement bar diameter	d_{bi}	20	mm	
Inner reinforcement bar spacing	S_{bi}	250	mm	
Calculated Layer Properties				
Height bottom of structure above rock	Y_b	42	m	
Height top of structure above rock	Y_t	46	m	
Ave shear modulus over structure ht.	G_s	44.3	MPa	$G_s = G_b/H(Y_t-Y_t^3/(3\ D^2)-Y_b+Y_b^3/(3\ D^2))$
Shear wave velocity at average G_s	v_s	149	m/s	$v_s = \mathrm{Sqrt}(G_s\ 1000/\rho_s)$
Calculated Frame Stiffness Properties				
Cracked wall moment of inertia	I_w	0.00267	m^4/m	
Cracked floor moment of inertia	I_f	0.00267	m^4/m	
Cracked roof moment of inertia	I_r	0.00267	m^4/m	
Wall stiffness	K_w	23529	kN m / m	$K_w = I_w\ E_c\ 1000/(H-\ t_r/2-\ t_f/2)$
Floor stiffness	K_f	23529	kN m / m	$K_f = I_f\ E_c\ 1000/(L-\ t_w)$
Roof stiffness	K_r	23529	kN m / m	$K_r = I_r\ E_c\ 1000/(L-\ t_w)$
Ratio roof / wall stiffness	r	1.0		
Ratio wall / roof stiffness	q	1.0		
Ratio floor / roof stiffness	j	1.0		
Structure flexibility	f_{si}	4.09E-05	m / kN / m	From Equation (5.4)
Assumed displacement ductility factor	μ_d	1.00		
Inelastic structure flexibility	f_{sii}	4.09E-05		$f_{sii} = f_{si}\ \mu_d$
Displaced soil block flexibility	f_s	2.26E-05	m / kN / m	From Equation (5.9)
Flexibility ratio	F_r	1.814		From Equation (5.8) Struct. Flexibility / Soil flex.

Table 7.1 Continued

Calculated EQ Interaction Parameters				
1-g free-field shear strain	ε_{f1}	0.0049		From Figure 5.3 for G_b = 150 MPa
1-g free-field strain corrected for G_b	ε_{fc}	0.0037		From Equation (5.3)
Design level peak ground acceln.	a_d	0.4	g	
Design level free-field shear strain	ε_{fd}	0.0015		$\varepsilon_{fd} = \varepsilon_{fc}\, a_d$
Interaction strain ratio	R_p	1.355		From Eq 5.10 (Penzien) Structure / Free-Field
Structure shear strain	ε_{st}	0.0020		$\varepsilon_{st} = \varepsilon_{fd}\, R_p$
Structure shear deflection	Δ_{st}	0.0076	m	$\Delta_{st} = \varepsilon_{st}\, H$
EQ moment at top corners	M_r	-157	kN m / m	Equation (6.2)
EQ moment at bottom corners	M_f	-157	kN m / m	Equation (6.1)
Correction factor for top moments	F_{mr}	1.05		From Figure 6.19
Correction factor for bottom moments	F_{mf}	1.14		From Figure 6.20
Corrected EQ mom. at top corners	M_{fc}	-165	kN m / m	$M_{fc} = M_r\, F_{mr}$
Corrected EQ mom. at bottom corners	M_{rc}	-178	kN m / m	$M_{rc} = M_f\, F_{mf}$
Equiv horizontal force at top structure	P	185	kN / m	$P = D_{st} / f_{si}$
Approx EQ axial force in wall	N_w	92	kN / m	$N_w = P/2\ (H - t_f/2 - t_r/2) / (L - t_w)$
Section Flexural Capacity				
Tensile strength of concrete in flexure	f_{tc}	3.75	MPa	Priestley et al page 267. Equation (5.3b)
Cracking moment of wall section	M_c	100	kN m / m	$M_c = 10^3\, f_{tc}\, t_w^2 / 6$
Ultimate strength tension on outside				
Reinforcement area per m length	A_s	2262	mm^2 / m	
Effective depth of section	d_e	0.348	m	$d_e = t_w - (c_s + d_b/2)/1000$
Compression width	a_{co}	32	mm	$a_{co} = (A_s\, f_y)/(0.85\, f_c\, 1000)$
Unreduced flexural capacity	M_u	***225***	***kN m / m***	No correction made for axial loads
Ultimate strength tension on inside				
Reinforcement area per m length	A_{si}	1257	mm^2 / m	
Effective depth of section	d_{ei}	0.350	m	$d_{ei} = t_w - (c_s + d_{bi}/2)/1000$
Compression width	a_{ci}	18	mm	$a_{ci} = (A_{si}\, f_y)/(0.85\, f_c\, 1000)$
Unreduced flexural capacity	M_{ui}	***129***	***kN m / m***	No correction made for axial loads
Approximate Gravity Load Moments				
Soil pressure on roof	p_r	78	kPa	$p_r = D_s\, \rho_s\, 9.81$
Weight of structure	w_{st}	131	kN / m	$w_{st} = 24\ (2\ H\ t_w + (L - 2t_w)(t_f + t_r))$
Soil pressure on base	p_f	113	kPa	$p_f = p_r + w_{st}/L$
Gravity load axial forces in walls	N_d	167	kN / m	Twice magnitude of EQ axial forces
Gravity load moment at top wall	M_{gt}	57	kN m / m	From frame analysis (+ve sign = clockwise)
Gravity load moment bottom wall	M_{gb}	-84	kN m / m	From frame analysis
Combined EQ + Gravity Load				
E + G Moment top left wall	M_{ctl}	-108	kN m / m	Tension on inside
E + G Moment top right wall	M_{ctr}	-222	kN m / m	Tension on outside
E + G Moment bottom left wall	M_{cbl}	-262	kN m / m	Tension on outside. Plastic hinge forms
E + G Moment bottom right wall	M_{cbr}	-94	kN m / m	Tension on inside
Approximate Yield Displacement				
Diff. between M_{cbl} and capacity	M_{dif}	-37	kN m / m	$M_{dif} = M_{cbl} + M_u$
Shear deflection of structure at yield	Δ_y	6.0	mm	Taken as defln when 1st plastic hinge forms
Required ductility factor	μ_{dr}	1.26		Only subjected to small inelastic displacement

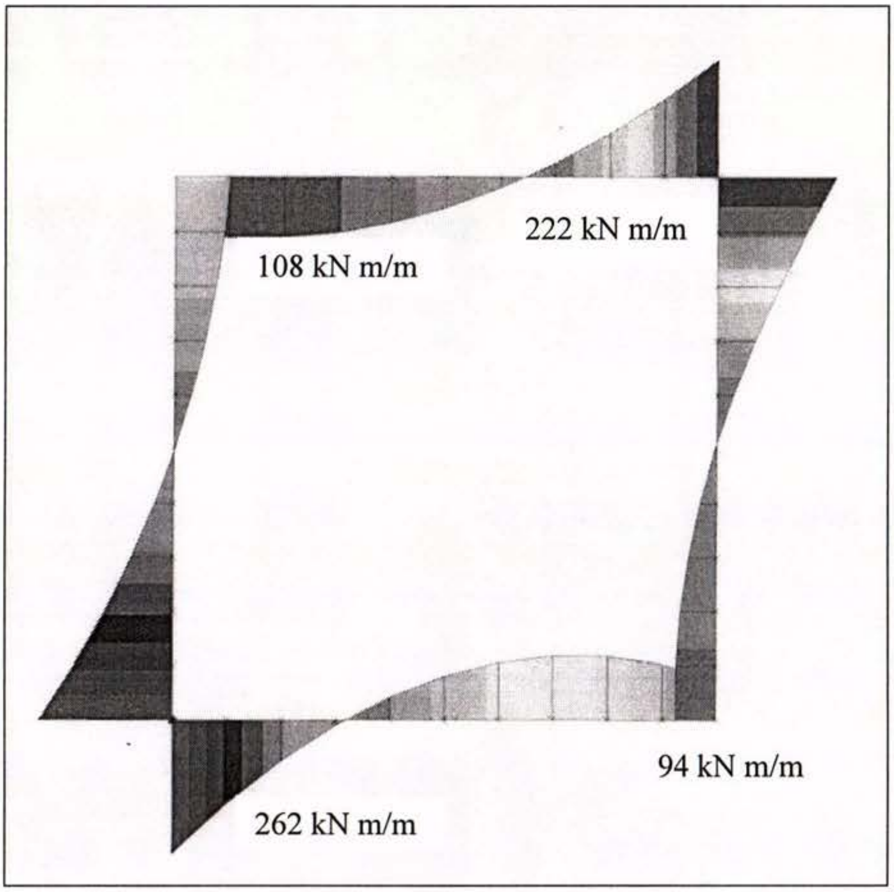

Figure 7.2. Combined earthquake induced + gravity bending moments

7.2 Box Subway Example

For the second example, the structure analysed in Section 7.1 was modified by reducing the wall thickness to a uniform 300 mm and also the quantity of the reinforcing. Other details of the structure and soil were maintained the same as previously. Reinforcement details for this modified box structure are listed in Table 7.2. The modified structure has dimensions typical of a pedestrian subway constructed above the water table.

Preliminary analyses indicated that this structure would be deformed into the inelastic range. For this case the previous analysis procedure developed for a structure responding elastically needs to be modified into a three-stage analysis procedure. The three stages are as follows:

1. The first stage is to calculate the ground motion acceleration required to induce yielding in the structure. The procedure is similar to that described in the first example except that the acceleration level is gradually increased (using the spreadsheet) until the first plastic hinge develops in the structure (assumed to be the yield level). This analysis is outlined in Table 7.2. An acceleration of 0.23 g resulted in yield. The corresponding shear displacement of the structure was 5.3 mm.
2. The second stage involves a pushover type frame analysis of the structure without the soil to determine the lateral force versus shear deflection relationship into the full inelastic displacement region. This analysis is required to define the overall structure stiffness or flexibility to use in the soil-structure interaction equations when the soil induced deformations exceed the structure yield displacement levels. For simplicity in the present analysis, an elasto-plastic force relationship was assumed in which the structure becomes fully plastic with no rise in the applied lateral force level beyond the yield displacement level. This relationship is illustrated in Figure 7.3. For these simplifying assumptions, the effective structure flexibility beyond the yield displacement level is the elastic flexibility multiplied by the ductility factor.
3. The third stage is to calculate the inelastic displacement and the ductility demand on the structure at the 0.4 g design ground acceleration. To carry out this part of the analysis the same spreadsheet used previously for the first stage can be used as shown in Table 7.3. The procedure is to estimate a ductility factor and then calculate the structure flexibility. Undertaking the standard soil-structure interaction analysis with the modified inelastic flexibility provides an estimate of the shear displacement in the structure. From this displacement and the yield displacement calculated in the first stage a ductility factor can be calculated. This factor is then used to improve the estimated ductility factor and the analysis repeated iteratively on the spreadsheet until convergence. The earthquake moments shown in Table 7.3 are incorrect for his inelastic stage of the analysis, but for convenience have been left in the table. Correct moments in the box section for inelastic response can only be reliably obtained by a detailed pushover analysis.

The procedure above indicates that under the 0.4 g design ground acceleration level the displacement ductility demand on the subway box will be about 2.0. There would be no

Table 7.2 Single-Barrel Box Subway Structure Example: Yield Displacement Calculation

Item	Symbol	Value	Units	Comments or Formula
Soil Input Parameters				
Soil layer depth	D	50	m	
Soil cover depth over structure	D_s	4.0	m	
Shear modulus at base of soil layer	G_b	200	MPa	Layer assumed to have parabolic varation of G
Soil density	ρ_s	2.0	t/m^3	
Soil Poisson's Ratio	ν	0.4		
Structure Geometric Inputs				
Outside height (overall)	H	3.6	m	
Outside length (overall)	L	3.6	m	
Floor thickness	t_f	0.30	m	
Roof thickness	t_r	0.30	m	
Wall thickness	t_w	0.30	m	
Concrete Section Inputs				
Young's modulus for concrete	E_c	30000	MPa	
Concrete crushing strength	f_c	25	MPa	
Reinforcement yield stress	f_y	300	MPa	
Cracked section MOI reduct. factor	F_{cs}	0.50		
Concrete cover to reinforcement	c_s	40	mm	
Outer reinforcement bar diameter	d_b	20	mm	
Outer reinforcement bar spacing	S_b	150	mm	
Inner reinforcement bar diameter	d_{bi}	20	mm	
Inner reinforcement bar spacing	S_{bi}	300	mm	
Calculated Layer Properties				
Height bottom of structure above rock	Y_b	42	m	
Height top of structure above rock	Y_t	46	m	
Ave shear modulus over structure ht.	G_s	43.6	MPa	$G_s = G_b/H(Y_t - Y_t^3/(3\ D^2) - Y_b + Y_b^3/(3\ D^2))$
Shear wave velocity at average G_s	v_s	148	m/s	$v_s = \mathrm{Sqrt}(G_s\ 1000/\rho_s)$
Calculated Frame Stiffness Properties				
Cracked wall moment of inertia	I_w	0.00113	m^4/m	
Cracked floor moment of inertia	I_f	0.00113	m^4/m	
Cracked roof moment of inertia	I_r	0.00113	m^4/m	
Wall stiffness	K_w	10227	kN m / m	$K_w = I_w\ E_c\ 1000/(H - t_r/2 - t_f/2)$
Floor stiffness	K_f	10227	kN m / m	$K_f = I_f\ E_c\ 1000/(L - t_w)$
Roof stiffness	K_r	10227	kN m / m	$K_r = I_r\ E_c\ 1000/(L - t_w)$
Ratio roof / wall stiffness	r	1.0		
Ratio wall / roof stiffness	q	1.0		
Ratio floor / roof stiffness	j	1.0		
Structure flexibility	f_{si}	8.87E-05	m / kN / m	From Equation (5.4)
Assumed displacement ductility factor	μ_d	1.00		Taken as 1.0 to calculate yield disp.
Inelastic structure flexibility	f_{sii}	8.87E-05		$f_{sii} = f_{si}\ \mu_d$
Displaced soil block flexibility	f_s	2.29E-05	m / kN / m	From Equation (5.9)
Flexibility ratio	F_r	3.87		From Equation (5.8) Struct. Flexibility / Soil flex.

Table 7.2 Continued

Calculated EQ Interaction Parameters				
1-g free-field shear strain	ε_{f1}	0.0049		From Figure 5.3 for G_b = 150 MPa
1-g free-field strain corrected for G_b	ε_{fc}	0.0037		From Equation (5.3)
Yield level peak ground acceln.	a_d	0.228	g	Increase until plastic hinge forms
Design level free-field shear strain	ε_{fd}	0.0008		$\varepsilon_{fd} = \varepsilon_{fc}\, a_d$
Interaction strain ratio	R_p	1.76		From Eq 5.10 (Penzien) Structure / Free-Field
Structure shear strain	ε_{st}	0.0015		$\varepsilon_{st} = \varepsilon_{fd}\, R_p$
Structure shear deflection	Δ_{st}	0.0053	m	$\Delta_{st} = \varepsilon_{st}\, H$
EQ moment at top corners	M_r	-49	kN m / m	Equation (6.2)
EQ moment at bottom corners	M_f	-49	kN m / m	Equation (6.1)
Correction factor for top moments	F_{mr}	1.16		From Figure 6.19
Correction factor for bottom moments	F_{mf}	1.29		From Figure 6.20
Corrected EQ mom. at top corners	M_{fc}	-57	kN m / m	$M_{fc} = M_r\, F_{mr}$
Corrected EQ mom. at bottom corners	M_{rc}	-64	kN m / m	$M_{rc} = M_f\, F_{mf}$
Equiv horizontal force at top structure	P	60	kN / m	$P = D_{st} / f_{si}$
Approx EQ axial force in wall	N_w	30	kN / m	$N_w = P/2\ (H - t_f/2 - t_r/2) / (L - t_w)$
Section Flexural Capacity				
Tensile strength of concrete in flexure	f_{tc}	3.75	MPa	Priestley et al page 267. Equation (5.3b)
Cracking moment of wall section	M_c	56	kN m / m	$M_c = 10^3 f_{tc}\, t_w^2 / 6$
Ultimate strength tension on outside				
Reinforcement area per m length	A_s	2094	mm^2 / m	
Effective depth of section	d_e	0.250	m	$d_e = t_w - (c_s + d_b/2)/1000$
Compression width	a_{co}	30	mm	$a_{co} = (A_s\, f_y)/(0.85\, f_c\, 1000)$
Unreduced flexural capacity	$\boldsymbol{M_u}$	***148***	***kN m / m***	No correction made for axial loads
Ultimate strength tension on inside				
Reinforcement area per m length	A_{si}	1047	mm^2 / m	
Effective depth of section	d_{ei}	0.250	m	$d_{ei} = t_w - (c_s + d_{bi}/2)/1000$
Compression width	a_{ci}	15	mm	$a_{ci} = (A_{si}\, f_y)/(0.85\, f_c\, 1000)$
Unreduced flexural capacity	$\boldsymbol{M_{ui}}$	***76***	***kN m / m***	No correction made for axial loads
Approximate Gravity Load Moments				
Soil pressure on roof	p_r	78	kPa	$p_r = D_s\, \rho_s\, 9.81$
Weight of structure	w_{st}	95	kN / m	$w_{st} = 24\ (2\ H\ t_w + (L - 2t_w)(t_f + t_r))$
Soil pressure on base	p_f	105	kPa	$p_f = p_r + w_{st}/L$
Gravity load axial forces in walls	N_d	154	kN / m	Twice magnitude of EQ axial forces
Gravity load moment at top wall	M_{gt}	57	kN m / m	From frame analysis (+ve sign = clockwise)
Gravity load moment bottom wall	M_{gb}	-84	kN m / m	From frame analysis
Combined EQ + Gravity Load				
E + G Moment top left wall	M_{ctl}	0	kN m / m	Tension on inside.
E + G Moment top right wall	M_{ctr}	-114	kN m / m	Tension on outside.
E + G Moment bottom left wall	M_{cbl}	-148	kN m / m	Tension on outside.
E + G Moment bottom right wall	M_{cbr}	20	kN m / m	Tension on inside.
Approximate Yield Displacement				
Diff. between M_{cbl} and capacity	M_{dif}	0.0	kN m / m	$M_{dif} = M_{cbl} + M_u$
Shear deflection of structure at yield	Δ_y	5.3	mm	Taken as defln when 1st plastic hinge forms
Required ductility factor	μ_{dr}	1.00		

Table 7.3 Single-Barrel Box Subway Structure Example: Approximate Ductility Factor Calculation

Item	Symbol	Value	Units	Comments or Formula
Soil Input Parameters				
Soil layer depth	D	50	m	
Soil cover depth over structure	D_s	4.0	m	
Shear modulus at base of soil layer	G_b	200	MPa	Layer assumed to have parabolic varation of G
Soil density	ρ_s	2.0	t/m^3	
Soil Poisson's Ratio	ν	0.4		
Structure Geometric Inputs				
Outside height (overall)	H	3.6	m	
Outside length (overall)	L	3.6	m	
Floor thickness	t_f	0.30	m	
Roof thickness	t_r	0.30	m	
Wall thickness	t_w	0.30	m	
Concrete Section Inputs				
Young's modulus for concrete	E_c	30000	MPa	
Concrete crushing strength	f_c	25	MPa	
Reinforcement yield stress	f_y	300	MPa	
Cracked section MOI reduct. factor	F_{cs}	0.50		
Concrete cover to reinforcement	c_s	40	mm	
Outer reinforcement bar diameter	d_b	20	mm	
Outer reinforcement bar spacing	S_b	150	mm	
Inner reinforcement bar diameter	d_{bi}	20	mm	
Inner reinforcement bar spacing	S_{bi}	300	mm	
Calculated Layer Properties				
Height bottom of structure above rock	Y_b	42	m	
Height top of structure above rock	Y_t	46	m	
Ave shear modulus over structure ht.	G_s	43.6	MPa	$G_s = G_b/H(Y_t-Y_t^3/(3\ D^2)-Y_b+Y_b^3/(3\ D^2))$
Shear wave velocity at average G_s	v_s	148	m/s	$v_s = \mathrm{Sqrt}(G_s\ 1000/\rho_s)$
Calculated Frame Stiffness Properties				
Cracked wall moment of inertia	I_w	0.00113	m^4/m	
Cracked floor moment of inertia	I_f	0.00113	m^4/m	
Cracked roof moment of inertia	I_r	0.00113	m^4/m	
Wall stiffness	K_w	10227	kN m / m	$K_w = I_w\ E_c\ 1000/(H- t_r/2- t_f/2)$
Floor stiffness	K_f	10227	kN m / m	$K_f = I_f\ E_c\ 1000/(L- t_w)$
Roof stiffness	K_r	10227	kN m / m	$K_r = I_r\ E_c\ 1000/(L- t_w)$
Ratio roof / wall stiffness	r	1.0		
Ratio wall / roof stiffness	q	1.0		
Ratio floor / roof stiffness	j	1.0		
Structure flexibility	f_{si}	8.87E-05	m / kN / m	From Equation (5.4)
Assumed displacement ductility factor	μ_d	2.03		Need to adjust by iterations
Inelastic structure flexibility	f_{sii}	1.80E-04		$f_{sii} = f_{si}\ \mu_d$
Displaced soil block flexibility	f_s	2.29E-05	m / kN / m	From Equation (5.9)
Flexibility ratio	F_r	7.86		From Equation (5.8) Struct. Flexibility / Soil flex.

Table 7.3 Continued

Calculated EQ Interaction Parameters				
1-g free-field shear strain	ε_{f1}	0.0049		From Figure 5.3 for G_b = 150 MPa
1-g free-field strain corrected for G_b	ε_{fc}	0.0037		From Equation (5.3)
Design level peak ground acceln.	a_d	0.4	g	
Design level free-field shear strain	ε_{fd}	0.0015		$\varepsilon_{fd} = \varepsilon_{fc}\, a_d$
Interaction strain ratio	R_p	2.04		From Eq 5.10 (Penzien) Structure / Free-Field
Structure shear strain	ε_{st}	0.0030		$\varepsilon_{st} = \varepsilon_{fd}\, R_p$
Structure shear deflection	Δ_{st}	0.0108	m	$\Delta_{st} = \varepsilon_{st}\, H$
EQ moment at top corners	M_r	-100	kN m / m	Equation (6.2)
EQ moment at bottom corners	M_f	-100	kN m / m	Equation (6.1)
Correction factor for top moments	F_{mr}	1.38		From Figure 6.19
Correction factor for bottom moments	F_{mf}	1.59		From Figure 6.20
Corrected EQ mom. at top corners	M_{fc}	-138	kN m / m	$M_{fc} = M_r\, F_{mr}$
Corrected EQ mom. at bottom corners	M_{rc}	-159	kN m / m	$M_{rc} = M_f\, F_{mf}$
Equiv horizontal force at top structure	P	121	kN / m	$P = D_{st} / f_{si}$
Approx EQ axial force in wall	N_w	61	kN / m	$N_w = P/2\ (H - t_f/2 - t_r/2) / (L - t_w)$
Section Flexural Capacity				
Tensile strength of concrete in flexure	f_{tc}	3.75	MPa	Priestley et al page 267. Equation (5.3b)
Cracking moment of wall section	M_c	56	kN m / m	$M_c = 10^3\, f_{tc}\, t_w^2 / 6$
Ultimate strength tension on outside				
Reinforcement area per m length	A_s	2094	mm^2 / m	
Effective depth of section	d_e	0.250	m	$d_e = t_w - (c_s + d_b/2)/1000$
Compression width	a_{co}	30	mm	$a_{co} = (A_s\, f_y)/(0.85\, f_c\, 1000)$
Unreduced flexural capacity	M_u	***148***	***kN m / m***	No correction made for axial loads
Ultimate strength tension on inside				
Reinforcement area per m length	A_{si}	1047	mm^2 / m	
Effective depth of section	d_{ei}	0.250	m	$d_{ei} = t_w - (c_s + d_{bi}/2)/1000$
Compression width	a_{ci}	15	mm	$a_{ci} = (A_{si}\, f_y)/(0.85\, f_c\, 1000)$
Unreduced flexural capacity	M_{ui}	***76***	***kN m / m***	No correction made for axial loads
Approximate Gravity Load Moments				
Soil pressure on roof	p_r	78	kPa	$p_r = D_s\, \rho_s\, 9.81$
Weight of structure	w_{st}	95	kN / m	$w_{st} = 24\ (2\ H\ t_w + (L - 2t_w)(t_f + t_r))$
Soil pressure on base	p_f	105	kPa	$p_f = p_r + w_{st}/L$
Gravity load axial forces in walls	N_d	154	kN / m	Twice magnitude of EQ axial forces
Gravity load moment at top wall	M_{gt}	57	kN m / m	From frame analysis (+ve sign = clockwise)
Gravity load moment bottom wall	M_{gb}	-84	kN m / m	From frame analysis
Combined EQ + Gravity Load				
E + G Moment top left wall	M_{ctl}	-81	kN m / m	Tension on inside. Plastic hinge forms
E + G Moment top right wall	M_{ctr}	-195	kN m / m	Tension on outside. Plastic hinge forms
E + G Moment bottom left wall	M_{cbl}	-243	kN m / m	Tension on outside. Plastic hinge forms
E + G Moment bottom right wall	M_{cbr}	-75	kN m / m	Tension on inside. Plastic hinge forms
Approximate Yield Displacement				
Diff. between M_{cbl} and capacity	M_{dif}	-95	kN m / m	$M_{dif} = M_{cbl} + M_u$
Shear deflection of structure at yield	Δ_y	5.3	mm	From elastic analysis in Table 7.3
Required ductility factor	μ_{dr}	2.03		Significant inelastic displacement occurs

difficulty in designing to achieve this level of structural ductility but a detailed design of the joints would be required to prevent serious damage. To obtain good levels of ductility the design criteria of Fenwick and Deam (2002) for corners between walls and slabs can be applied.

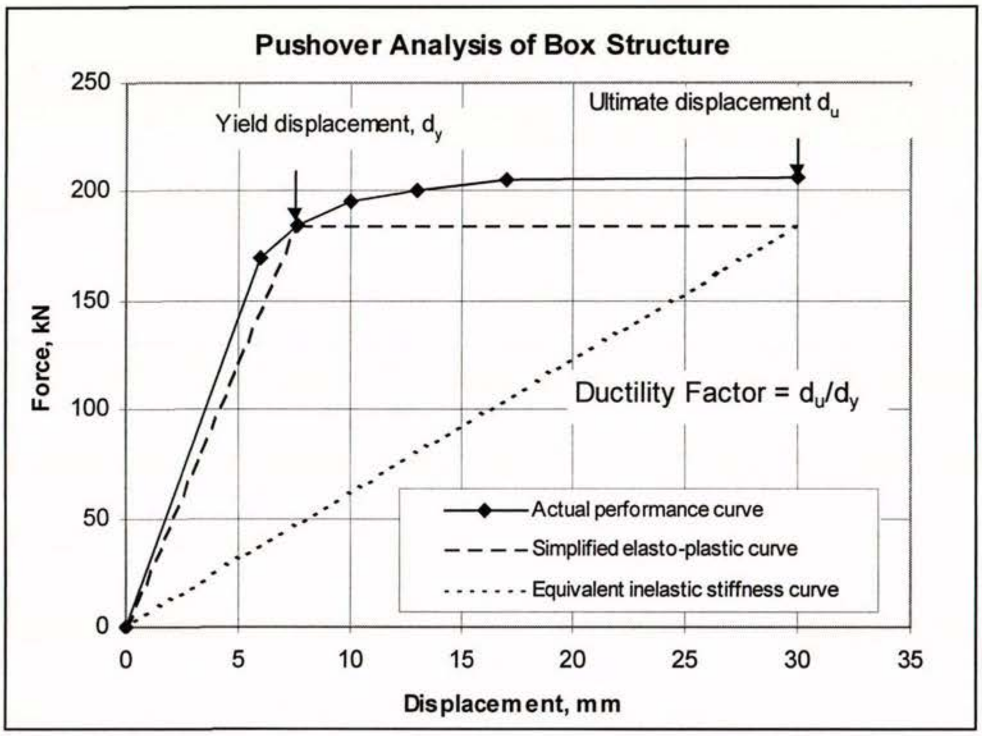

Figure 7.3 Pushover analysis and idealised elasto-plastic response.

8. CONCLUSIONS

(a) The empirical relationship developed by Wang (1993) for assessing the racking interaction of rectangular section structures with the surrounding soil during earthquakes was verified by undertaking a large number of simplified dynamic finite element analyses and by comparison with analytical expressions recently published. Agreement between the various relationships was found to be adequate for structural design purposes and in general the design approach developed by Wang (1993) was found to be applicable under most conditions likely to be encountered in practise.

(b) The work of Wang was extended by undertaking a large number of simplified dynamic finite element analyses to determine the sensitivity of the interaction curves to variations in the main parameters. This produced a number of charts that can be used in the earthquake design of smaller underground structures where the site information is unlikely to be known in sufficient detail to warrant more sophisticated analyses. Charts were prepared for estimating the free-field soil strains and the magnitude of the internal force actions in the cross-section of the structure. Reliable simple methods of estimating these parameters have not been previously published.

(c) The finite element method developed for the present study can also be used to analyse directly large or more complex structures when more detailed site information is likely to be available.

(d) Application of the Wang design method to several box culverts and pedestrian subway structures showed that the internal forces from earthquake induced raking deformations can be large in comparison to actions produced by gravity and water pressure loads. These earthquake-induced actions need to be considered in the design of most rectangular underground structures.

(e) A displacement based design approach is required when the structure is loaded beyond yield levels by the earthquake induced ground deformations. The design process in this case is rather more complex involving the need for a simple pushover analysis to determine the structure post-elastic stiffness or flexibility. An example was presented which outlined a method of determining the ductility demand on the structure when inelastic deformation was significant.

9. ACKNOWLEDGEMENT

Financial support from the Earthquake Commission Research Foundation to undertake this project is gratefully acknowledged.

10. REFERENCES

Brunsdon D R, (1999), Personal Communication

Dowding C H, Rozen A, (1978) *"Damage to Rock Tunnels from Earthquake Shaking"*, Journal of the Geotechnical Engineering Division, ASCE, Vol. 104, No. GT2, February 1978.

Fenwick R and Deam B (2002) *"Design of Opening Corners Between Reinforced Concree Walls and Slabs"*, SESOC Journal (NZ), Vol 16, No 1, April 2003.

Hwang R N, and Lysmer J, (1981) *"Response of Buried Structures to Traveling Waves"*, Journal of the Geotechnical Engineering Division, ASCE, Vol. 107, No. GT2, February, 1981.

Iwatate T, Kobayashi Y,Kusu H and Rin K, (2000), *"Investigation and Shaking Table Tests of Subway Structures of the Hyogoken-Nanbu Earthquake"*. Proceedings 12th World Conference on Earthquake Engineering, Auckland.

Kuesel T R, (1969) *"Earthquake Design Criteria for Subways"*, Journal of the Structural Divisions, ASCE, Vol 95, No ST6, June 1969.

Lew H S, Leyendecker E V, and Dickers R D, (1971), *"Engineering aspects of the 1971 San Fernando Earthquake"*. Building Science Series 40, US Dept of Commerce, NBS.

Monsees J E, and Merritt J L, (1991) *"Earthquake Considerations in Design of the Los Angeles Metro"*, ASCE Conference on Lifeline Earthquake Engineering, 1991.

Nishiyama S, Kawama I, Muroya K, Haya H, and Nishimura A, (2000), *"Experimental Study of Seismic Behavior of Box Type Tunnel Constructed by Open Cutting Method"*. Proceedings 12th World Conference on Earthquake Engineering, Auckland.

Nishioka T, and Unjoh S, (2002) *"A Simplified Seismic Design Method for Underground Structures Based on Shear Strain Transmitting Characteristics"*, SEWC 2002, Yokohama Japan.

Nishioka T, and Unjoh S, (2003) *"A Simplified Evaluation Method for the Seismic of Undreground Common Utility Boxes"*, Proceedings 2003 Pacific Conference on Earthquake Engineering, Auckland.

Owen G N, and Scholl, R E (1981) *"Earthquake Engineering of Large Underground Structures"*, prepared for the Federal Highway Administration, FHWAIRD-801195.

Penzien J, (2000) *"Seismically Induced Racking of Tunnel Linings"*, Earthquake Engineering and Structural Dynamics, Vol 29:683-691.

Penzien J, and Wu C L, (1998) *"Stresses in Linings of Bored Tunnels"* , Earthquake Engineering and Structural Dynamics, Vol 27: 283-300.

Priestley M J N, Davidson B J, Honey G D, Hopkins D C, Martin R J, Ramsay G, Vessey J V, and Wood J H, (1986), *"Seismic Design of Storage Tanks"*, Recommendation of a Study Group of NZNSEE.

Priestley M J N, Siebel F and Calvi G M, (1996), *"Seismic Design and Retrofit of Bridges"*, John Wiley & Sons Inc, New York.

Public Works Research Institute, (1996) *"Report on the Disaster Caused by the 1995 Hyogoken Nanbu Earthquake"*, PWRI, Ministry of Construction, Vol 196, 455-470.

Sharma S, and Judd W R, (1991) *"Underground Opening Damage from Earthquakes"*, Engineering Geology, 30, 1991.

Shepherd R, and Wood J H (1966) *"Normal Mode Properties of Multi-Storey Frameworks"*, Journal of Sound and Vibration, Vol 3, No 3, 300-314.

Transit New Zealand, (2003) *"Bridge Manual"*, SP/M/014, Wellington.

Wang J M, (1985 *"The Distribution of Earthquake Damage to Underground Facilities during the 1976 Tangshan Earthquake"*, Earthquake Spectra, Vol 1, No 4, 1985.

Wang J (1993), *"Seismic Design of Tunnels"*, Monograph 7, Parsons Brinckerhoff Quade & Douglas Inc, New York, June 1993.

Wood J H, (1973) "Earthquake- Induced Soil Pressures on Structures", EERL 73-05, Earthquake Engineering Research Laboratory, California Institute of Technology.

Wood J H, and Jenkins D A, (2000), *"Seismic Analysis of Buried Arch Structures"*. Proceedings 12th World Conference on Earthquake Engineering, Auckland, February, 2000.